



National Aeronautics and
Space Administration

TechBriefs



Electronic Components and Circuits



Electronic Systems



Physical Sciences



Materials



Computer Programs



Mechanics



Machinery



Fabrication Technology



Mathematics and Information Sciences



Life Sciences

COMPLETED

INTRODUCTION

Tech Briefs are short announcements of new technology derived from the research and development activities of the National Aeronautics and Space Administration. These Briefs emphasize information considered likely to be transferable across industrial, regional, or disciplinary lines and are issued to encourage commercial application.

Availability of NASA Tech Briefs and TSP's

Distribution of NASA Tech Briefs, a monthly periodical publication, is limited to engineers in U.S. industry and to other domestic technology transfer agents. Requests for individual Tech Briefs or for Technical Support Packages (TSP's) announced herein should be addressed to

NASA Center for AeroSpace Information
Technology Transfer Office
800 Elkridge Landing Rd.
Linthicum Heights, MD 21090-2934
Telephone No. (301) 621-0245

Please reference the three-letter, five-digit control number located at the end of each Tech Brief. Information on NASA's Technology Utilization Program, its documents, and services is also available at the same facility.

Technology Utilization Officers and Patent Counsels are located at NASA field installations to provide technology-transfer access to industrial users. Inquiries can be made by writing to NASA field installations listed below.

Technology Utilization Officers and Patent Counsels

Ames Research Center
Technology Utilization Officer
Mail Code 223-3
Moffett Field, CA 94035

Patent Counsel
Mail Code 200-11
Moffett Field, CA 94035

Goddard Space Flight Center
Technology Utilization Officer
Mail Code 702-1
Greenbelt, MD 20771

Patent Counsel
Mail Code 204
Greenbelt, MD 20771

Lyndon B. Johnson Space Center
Technology Utilization Officer
Mail Code IC-4
Houston, TX 77058

Patent Counsel
Mail Code AL3
Houston, TX 77058

John F. Kennedy Space Center
Technology Utilization Officer
Mail Stop PT-PMO-A
Kennedy Space Center, FL 32899

Patent Counsel
Mail Code PT-PAT
Kennedy Space Center, FL 32899

Langley Research Center
Technology Utilization Officer
Mail Stop 143
Hampton, VA 23665

Patent Counsel
Mail Code 279
Hampton, VA 23665

Lewis Research Center
Technology Utilization Officer
Mail Stop 7-3
21000 Brookpark Road
Cleveland, OH 44135

Patent Counsel
Mail Code LE-LAW
21000 Brookpark Road
Cleveland, OH 44135

Jet Propulsion Laboratory
Technology Utilization Officer
Mail Stop 156-211
4800 Oak Grove Drive
Pasadena, CA 91109

NASA Resident Office-JPL
Technology Utilization Officer
Mail Stop 180-801
4800 Oak Grove Drive
Pasadena, CA 91109

Patent Counsel
Mail Code 180-801
4800 Oak Grove Drive
Pasadena, CA 91109

George C. Marshall Space Flight Center
Technology Utilization Officer
Code AT01
Marshall Space Flight Center,
AL 35812

Patent Counsel
Mail Code CC01
Marshall Space Flight Center,
AL 35812

John C. Stennis Space Center
Technology Utilization Officer
Code HA-30
Stennis Space Center, MS 39529

NASA Headquarters
Technology Utilization Officer
Code CU
Washington, DC 20546

Assistant General Counsel for Patent Matters
Code GP
Washington, DC 20546

Dryden Flight Research Center
Technology Utilization Officer
M/S D21-31
Bldg. 4832 Whse 7
Lilly Dr.
Edwards, CA 93523

BLANK PAGE



National Aeronautics and
Space Administration

TechBriefs

October 1998
98-10

5	Electronic Components and Circuits	
----------	---	---

17	Electronic Systems	
-----------	---------------------------	---

23	Physical Sciences	
-----------	--------------------------	---

27	Materials	
-----------	------------------	---

33	Computer Programs	
-----------	--------------------------	---

37	Mechanics	
-----------	------------------	---

43	Machinery	
-----------	------------------	---

47	Fabrication Technology	
-----------	-------------------------------	---

53	Mathematics and Information Sciences	
-----------	---	---

This document was prepared under the sponsorship of the National Aeronautics and Space Administration. Neither the United States Government nor any person acting on behalf of the United States Government assumes any liability resulting from the use of the information contained in this document, or warrants that such use will be free from privately owned rights.

BLANK PAGE



Electronic Components and Circuits

Hardware, Techniques, and Processes

- 7 Delta-Doped Hybrid Advanced Detector
- 8 Optimized Two-Wavelength Focal-Plane Arrays of QWIPs
- 9 System-Level Integrated Circuits for Phased-Array Antennas
- 10 Active-Pixel-Sensor Digital Camera on a Single Chip
- 11 Active-Pixel Sensors With "Winner-Take-All" Mode
- 12 Monolithic GaAs FET Power Amplifiers for K_a Band
- 13 Augmented Active Pixel Sensors Would Compute Centers of Mass
- 14 Micromachined Magnetostatic Switches

BLANK PAGE

Delta-Doped Hybrid Advanced Detector

This device could detect both particles and photons over wide energy ranges.

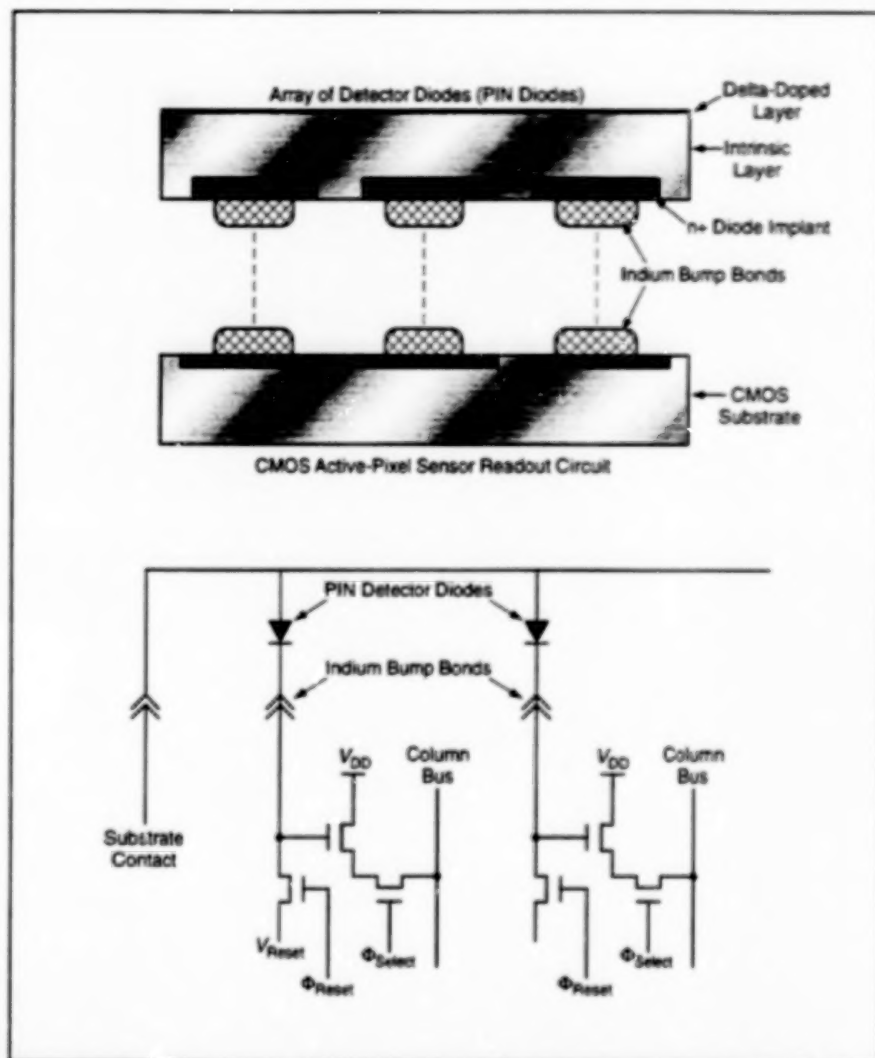
NASA's Jet Propulsion Laboratory,
Pasadena, California

The delta-doped hybrid advanced detector is a developmental integrated electronic imaging and detecting circuit designed to be sensitive to (1) charged particles with kinetic energies ranging from hundreds through millions of electron volts and (2) photons ranging from visible light to x rays. Heretofore, the lower kinetic-energy limit of detectability of charged particles has been about 10 keV. To extend the limit downward to hundreds of electron volts, the design of the delta-doped hybrid advanced detector calls for a combination of features from several recent lines of development of detector and readout circuits.

The detector would be a hybrid of (1) a square array of reverse-biased positive/intrinsic/negative (PIN) diodes with (2) a correspondingly patterned complementary metal oxide/semiconductor (CMOS) integrated readout circuit fabricated by a standard process. The array of PIN diodes would be electrically and mechanically connected to the readout circuit through indium bump bonds (see figure).

In a reverse-biased PIN diode, the applied electric field depletes the intrinsic region of charge carriers. When an energetic charged particle or photon of sufficient energy enters the depletion region, some or all of its energy is dissipated in the generation of electron-hole pairs, which are then swept out by the electric field and detected. However, low-energy particles typically do not penetrate to the intrinsic region in a conventional PIN diode. Instead, they tend to dissipate their energies in a "dead" layer near the surface through which they enter. The dead layer contains an undepleted, highly p- or n-doped, diode contact sublayer where electrons and holes recombine before they can be detected. The dead layer also contains a surface depletion sublayer with an electric field that (a) tends to confine some charge carriers until they recombine at the surface and (b) drives other charge carriers into the undepleted region, where they recombine before detection.

The delta-doping aspect of the delta-doped hybrid advanced detector would extend the low-energy detection limit by reducing the effect of the dead layer. Delta doping is so named because its density-vs.-depth characteristic is reminiscent of the Dirac δ function (impulse function). The dopant is concentrated in a very thin



Detector Diodes Would be Joined With CMOS Readout Circuitry by use of indium bump bonds. Pixels could be raster-scanned or read out nonsequentially. The column signal-processing circuitry would enable the incorporation of correlated double sampling or other advanced features.

layer (preferably, a single atomic layer). In the delta-doped hybrid advanced detector, the delta-doped layer would be placed within 5 or 10 Å of the detector surface. The delta-doped layer would provide a very thin undepleted region and surface depletion region, with a resultant dead-layer thickness of only 15 to 20 Å, making possible the collection of electrons and holes generated by low-energy charged particles and photons that can penetrate at least 20 Å or so.

Heretofore, delta doping has been used on charge-coupled devices (CCDs). Although CCDs could be used as detectors, they are relatively highly doped; it would be necessary to thin them to enable their charge-collecting depletion regions to

extend through the thickness. Thinning can be accomplished only by a difficult fabrication process step, and the remaining thickness is not sufficient for measuring the energies of x rays and high-energy particles that deposit charge carriers at great depths. Accordingly, the array of PIN diodes in the delta-doped hybrid advanced detector are made from a wafer of high-resistivity silicon [nominally intrinsic, though actually very lightly p-doped (to a concentration of 10^{12} cm^{-3})] like that used in silicon strip detectors. The use of this high-resistivity silicon makes thinning unnecessary, thereby making it possible to retain sufficient thickness for detection of highly energetic charged particles and photons.

The CMOS readout circuit would be of the active-pixel sensor (APS) type, offering enough sensitivity to enable resolution of the small signals generated by low-energy charged particles. This circuit would consume only milliwatts of power, in contradistinction to a CCD, which typically consumes watts. Moreover, whereas a CCD must be read out sequentially by rows and columns, the APS circuit would be capable of nonsequential readout of pixels, making it possible to use various advanced readout schemes. Like a CCD, this readout circuit could preserve the low capacitance of the detector diodes, with resultant readout noise of 10 electrons or less (vs. hundreds to thousands of electrons for a conventional strip detector).

A pixel-guarding technique would be used to preserve low effective input capacitances for the APS readout circuit, even in the presence of relatively large indium bump pads on the input nodes, thereby preserving the high conversion gain needed for high sensitivity and a high signal-to-noise ratio. In this technique, each bump bond would be connected to a source follower serving as a unity-gain buffer, the output of which would be fed to a metal guard electrode underneath the bump bond and separated from the bump bond by a thin insulating layer.

This work was done by Eric Fossum, Thomas Cunningham, Shouleh Nikzad, George Soli, and Bedabrata Pain of

Caltech for NASA's Jet Propulsion Laboratory. Further information is contained in a TSP [see page 1].

In accordance with Public Law 96-517, the contractor has elected to retain title to this invention. Inquiries concerning rights for its commercial use should be addressed to

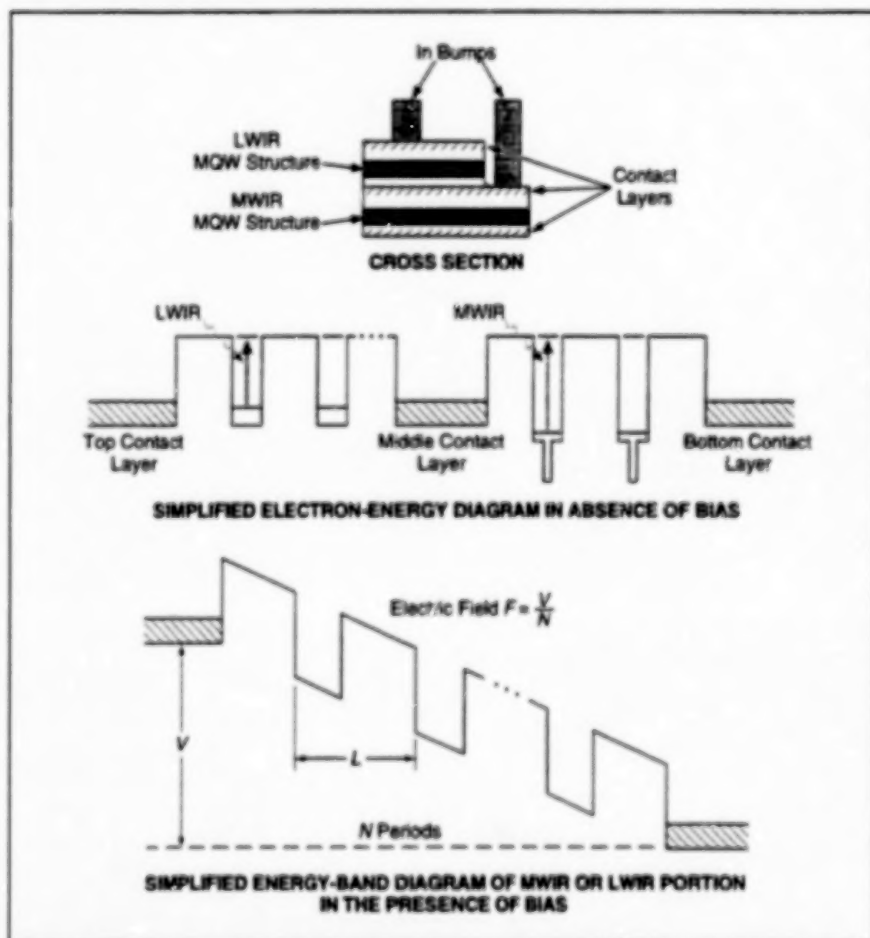
Technology Reporting Office
JPL
Mail Stop 122-116
4800 Oak Grove Drive
Pasadena, CA 91109
(818) 354-2240

Refer to NPO-20111, volume and number of this NASA Tech Briefs issue, and the page number.

Optimized Two-Wavelength Focal-Plane Arrays of QWIPs

Only one bias voltage would be needed for readout at both wavelengths.

NASA's Jet Propulsion Laboratory,
Pasadena, California



This Configuration and its Conduction-Band Electron-Energy Diagrams are typical for a device like that described in the text. The device would be grown by molecular-beam epitaxy onto a semi-insulating GaAs substrate. The contact layers would be made of heavily doped GaAs. Indium bumps would serve as contacts to external circuitry.

A concept for optimizing the designs of two-wavelength GaAs-based quantum-well infrared photodetectors (QWIPs) could make it practical to use focal-plane arrays of QWIPs as image sensors in two-wavelength infrared cameras. Potential applications for such cameras include surveillance, tracking of military targets, night vision, and thermal mapping. One important advantage of a two-wavelength over a one-wavelength camera is the possibility of using Planck's radiation law to calculate the temperature of an imaged object from the ratio between the brightnesses of the object at the two wavelengths.

Concepts for using focal-plane arrays of GaAs-based QWIPs in different configurations as two-wavelength infrared image sensors have been described in previous articles in NASA Tech Briefs. The present concept applies to a configuration in which each pixel in a focal-plane array would contain two stacked multiple-quantum-well (MQW) photodetectors. The energy depths of the wells, the geometric thicknesses of the wells, and the geometric thicknesses of the barriers between the wells in one MQW structure would be chosen to obtain peak response in the desired long-wavelength infrared (LWIR) band; the corresponding parameters for the other MQW structure would be chosen to obtain peak response in the desired medium-wavelength infrared (MWIR) band (see figure). Both MQW structures would be biased and read out simultaneously, but

independently of each other, through separate indium bump contacts connected to a readout multiplexer.

Research on previous designs based on this configuration has revealed two problems that until now have made it impractical to make a two-wavelength infrared camera. The first problem is that for simultaneous detection two-QWP stack in each pixel must be supplied with two different bias potentials, which cannot be obtained from any currently available readout multiplexers. The second problem is that in voltage-tunable design a high bias potential (>8 V) must be supplied to the LWIR QWP to switch on LWIR detection.

The present concept would make it possible to operate the QWPs with equal and lower bias potentials. The QWPs designed according to this concept would be at least as responsive as are those of older designs that require higher and unequal bias potentials. The concept involves the following reasoning: The need for different and higher bias voltages in older designs arises, in part, from fundamental physical mechanisms that make it necessary to use larger bias electric fields to detect photons of shorter wavelengths. One could obtain a given bias electric field at a lower bias potential by applying that potential across a lesser thickness of material, that is, across fewer quantum-well periods. For fundamental physical reasons, it turns out that the responsivity of an MQW device is inde-

pendent of the number of MQW periods (provided that the electric field remains the same), so that one has some design flexibility to decrease the number of MQW periods.

The relevant design parameters must satisfy the following equations:

$$F_L = V_L / N_L L_L \text{ and } F_W = V_W / N_W L_W$$

where F_L and F_W are the electric field needed for detection of LWIR and MWIR photons, respectively; V_L and V_W are the bias potential applied to the LWIR and MWIR structures, respectively; N_L and N_W are the number of spatial periods in the LWIR and MWIR MQW structures, respectively; and L_L and L_W are the depths of a quantum-well period of the LWIR and an MWIR MQW structures, respectively. Heretofore, one would typically choose $L_L = L_W$ and $N_L = N_W$, and choose two different bias potentials to obtain the required F_L and F_W . One can still choose $L_L = L_W$ while choosing different values of N_L and N_W to make it possible to use $V_L = V_W$ to obtain the required F_L and F_W . The required values of N_L and N_W would then be related by

$$F_L N_L = F_W N_W$$

To obtain reasonably high responsivity from each stack, $F_W > F_L$ is required. Thus, the obvious choice would be $N_L > N_W$. It is also worth noting that the total number of periods in the structure ($N_L + N_W$) is limited by the molecular-beam-epitaxy (MBE)

growth time because it tends to increase the number of defects with the increasing growth time. Therefore, one has to increase N_L and decrease N_W from their values being equal. Although, this choice would result in a decrease in LWIR noise current and increase in MWIR noise current, the noise current of the LWIR QWP is still higher than that of the MWIR QWP. This is because dark current of the LWIR QWP is few orders larger than that of MWIR QWP. Therefore, overall performance of the two-wavelength QWP will be enhanced.

This work was done by Sumith Bandiera, Sarath Gunapala, and John K. Liu of Caltech for NASA's Jet Propulsion Laboratory. Further information is contained in JPL TSP [see page 1].

In accordance with Public Law 96-517, the contractor has elected to retain title to this invention. Inquiries concerning rights for its commercial use should be addressed to

Technology Reporting Office
JPL
Mail Stop 122-116
4800 Oak Grove Drive
Pasadena, CA 91109
(818) 354-2240

Refer to NPO-20279, volume and number of this NASA Tech Briefs issue, and the page number.

System-Level Integrated Circuits for Phased-Array Antennas

Support and interface circuits are merged with RF components in advanced MMIC units.

Lewis Research Center,
Cleveland, Ohio

Modules of electronic circuitry that perform the amplitude- and phase-control and the status-monitoring functions for eight-element (2×4) subarrays of K-band phased-array antennas have been developed as prototype building blocks for future phased-array antennas. These modules are characterized as, among other things, system-level integrated circuits (SLICs) because they reach a new level of functionality, previously achieved only by use of larger, heavier systems. This functionality is achieved through sophisticated design that incorporates monolithic microwave integrated circuits (MMICs) and other components and involves an unprecedented degree of integration of these components with regard, not only for electrical performance, but also for considerations as diverse as temperature control, size, weight, mass-pro-

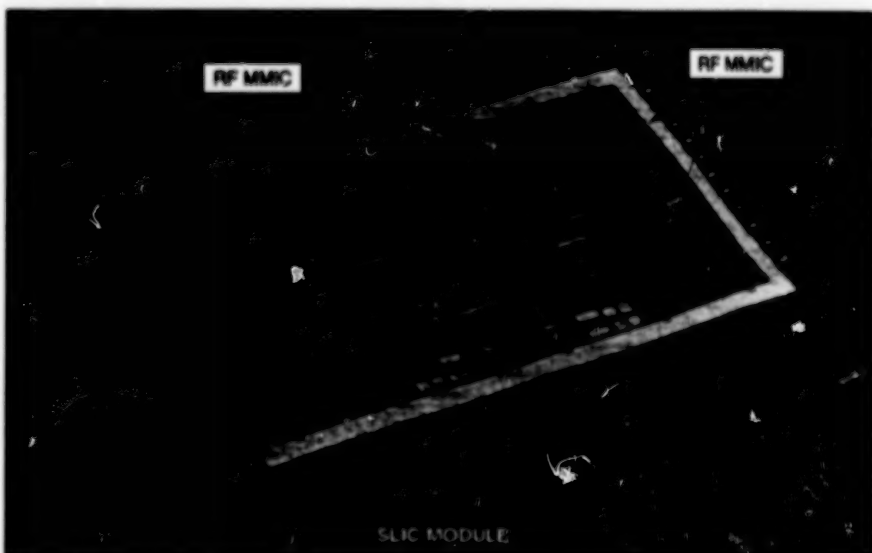


Figure 1. One Compact Package contains all the circuitry needed to set the amplitudes and phases of RF signals in eight antenna elements at commanded values.

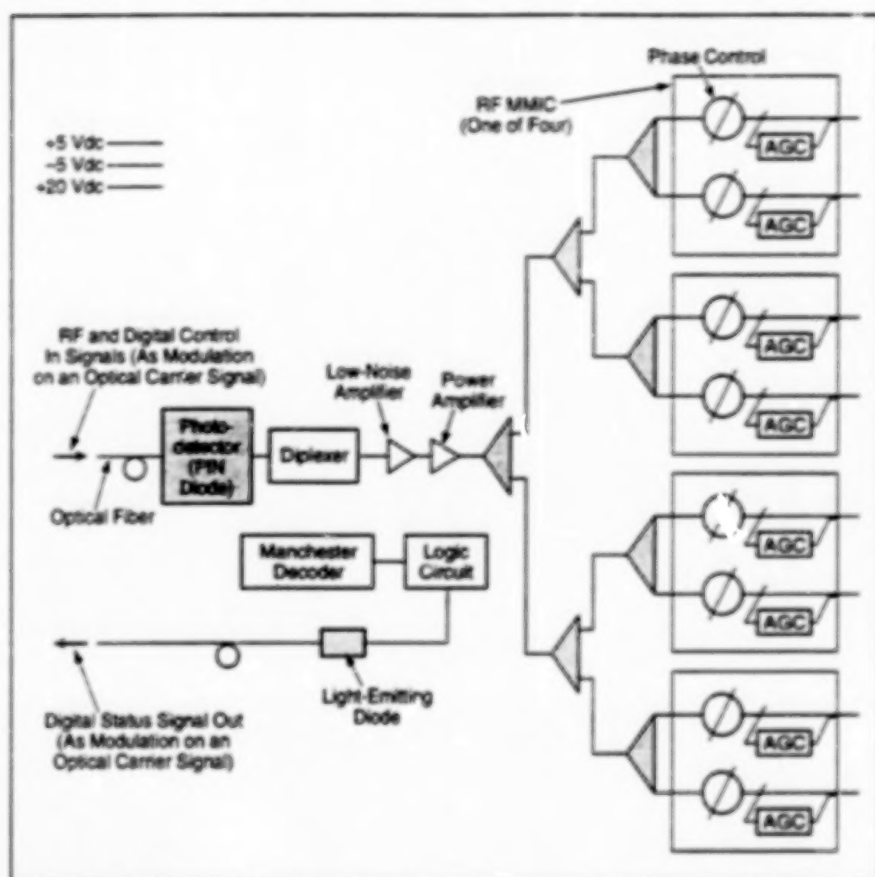


Figure 2. This Simplified Block Diagram represents the major functions of submodules of the module shown in Figure 1.

ducibility, reliability, cost, complexity of interconnections, and compatibility with other electronic equipment.

Exploiting recent advances in MMICs, photonics, and packaging, each SUC module contains optoelectronic and electronic support and interface components and circuits integrated directly with radio-

frequency (RF) components and circuits. Each SUC module (see Figure 1) comprises a tilelike array of MMIC submodules plus supporting control and signal-distribution elements. All of these components are integrated into a single thin, lightweight package by use of the microwave high-density interconnect

(M-HDI) process, which is the enabling process for making tilelike phased arrays with the desired level of calibration and control.

Among the submodules in each SUC module (see Figure 2) are four highly integrated dual-channel RF MMICs, each of which contains two phase shifters that operate under 3-bit digital control, two analog attenuators, shift registers for transmission of control data for adjustment of phases, analog automatic gain control (AGC) circuits, and status-monitoring circuits. Digital control signals and an RF signal are fed to the SUC module via a single photonic link. This combination of signals is detected by a positive/intrinsic/negative (PIN) diode in the module, then separated by other circuitry into control and RF components. The RF signal is amplified and split eight ways to feed the four dual-channel RF MMICs. A peak detector at the output terminal of each channel on each RF MMIC samples the output signal level; this level is compared with a commanded level in the corresponding AGC circuit, which adjusts the setting of an attenuator to maintain the channel output at the commanded level.

This work was done by John Windyka and Ed Zablocki of Sanders for Lewis Research Center. Further information is contained in a TSP (see page 1).

Inquiries concerning rights for the commercial use of this invention should be addressed to NASA Lewis Research Center, Commercial Technology Office, Attn: Tech Brief Patent Status, Mail Stop 7-3, 21000 Brookpark Road, Cleveland, Ohio 44135. Refer to LEW-16627.

Active-Pixel-Sensor Digital Camera on a Single Chip

The entire camera, exclusive of the optics, is only 1 cm³ (0.06 in.³).

The figure shows a complementary metal oxide/semiconductor (CMOS) integrated circuit that contains all of the electronic circuitry of a programmable active-pixel-sensor digital camera. Heretofore, digital cameras have been assembled from charge-coupled-device (CCD) chips, separate analog-to-digital converters, and separate units that perform timing, control, and interface functions; each unit adds to the size, cost, and power consumption of a camera. The present single-chip camera is a prototype developed for many applications within the space program. It also meets the demands of a large potential market for

compact, low-power-consumption, and (eventually) inexpensive portable digital cameras. The chip has been packaged as a low-power camera occupying only 1 cm³ (0.06 in.³), exclusive of optics, with an all-digital 5-wire serial interface. The chip is also being incorporated, along with a wireless interface unit, into a battery-operated camera with a volume of less than 32 cm³ (2 in.³).

Included on the chip are analog-to-digital converters (ADCs) and full timing, control, and interface circuitry. All analog reference voltages for imaging and digitization are generated by programmable digital-to-analog converters (DACs) that

are also included on the chip. Thus, the camera contains a complete digital interface. Through a single digital input pin, the chip can be programmed to perform a variety of imaging operations and/or to establish the required interface configuration; this capability facilitates integration with a variety of external digital systems.

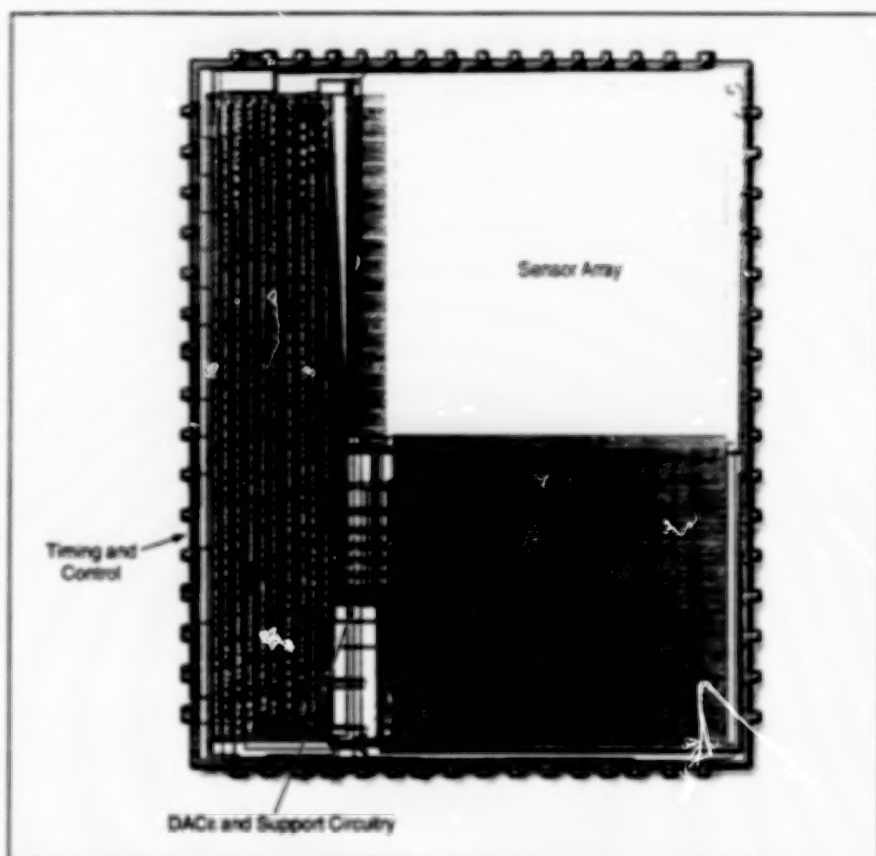
The image-sensor portion of the chip is a 256 × 256 array of photogate active pixel detector circuits, with a 20.4-μm pixel pitch and a 21-percent fill factor. Each pixel includes a source follower for coupling the pixel output to a column bus. Next to the sensor array is the array of ADCs, of which there are 256 in a column-

NASA's Jet Propulsion Laboratory,
Pasadena, California

parallel arrangement. Each ADC uses a successive approximation algorithm with internal correlated double-sampling and offset-correction circuits to reduce noise, designed to yield an output with 10 bits of resolution. To decrease power consumption while an image is not being acquired, the chip has a low-power (40- μ W) idle mode, in which the DACs, pixel source followers, and ADCs are disabled.

The chip can be programmed in order to set the desired exposure time and to operate in any of a number of imaging modes. The amount of data and power required for an image may be reduced by programming the chip to use a smaller window contained within the 256 x 256 array and by subsampling the pixels within the desired window. Although designed primarily to take still pictures, the chip can also be programmed to acquire images continuously. After acquiring a digital still image, the chip automatically enters the low-power idle mode.

The chip can be programmed to produce serial or parallel data output in a variety of formats. It can be made to implement full- or half-duplex protocols and to generate vertical and horizontal frame-synchronizing signals. It can accommodate a variety of input and output data rates and internal clock rates; it can even operate with separate input command and output data rates or receive asynchronous input command data at particular bit rates with no input clock. This flexibility is achieved by use of separate programmable clocks, derived internally from the input clock, to control various operations on the chip. The chip can support frame rates up to 14 Hz with serial output or 60 Hz with parallel output. During full operation with serial output, the total power consumed by



All the Electronic Circuitry of a Digital Camera fits in a rectangular area of 9.3 by 11.2 mm and consumes only milliwatts of power.

the chip is about 20 mW.

This work was done by Timothy Shaw, Bedabrata Pain, Brita Olson, Robert Nixon, Eric Fossum, Roger Panicecci, and Barmak Mansoorian of Caltech for NASA's Jet Propulsion Laboratory. Further information is contained in a TSP [see page 1].

In accordance with Public Law 96-517, the contractor has elected to retain title to this invention. Inquiries concern-

ing rights for its commercial use should be addressed to

Technology Reporting Office

JPL

Mail Stop 122-116

4800 Oak Grove Drive

Pasadena, CA 91109

(818) 354-2240

Refer to NPO-20262, volume and number of this NASA Tech Briefs issue, and the page number.

Active-Pixel Sensors With "Winner-Take-All" Mode

These sensors could function in either brightest-pixel or normal image-readout modes.

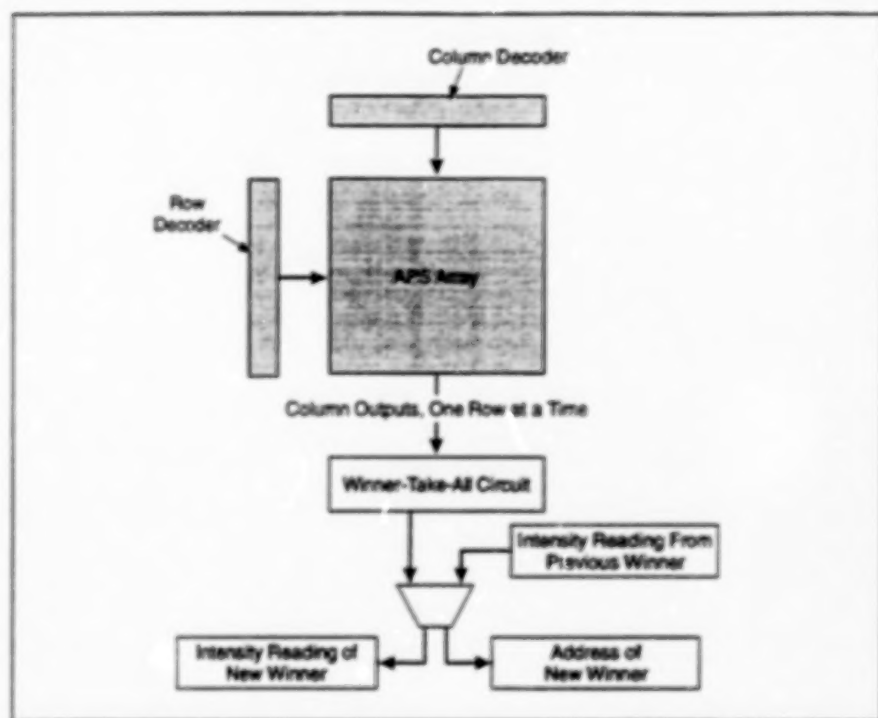
Circuits to generate the intensity reading and the coordinates of the brightest pixel in each image would be added to imaging photodetector arrays of the active-pixel-sensor (APS) type, according to a proposal. For a given APS, the additional circuitry for locating the brightest pixel would be installed at the periphery of the basic APS circuit. The additional circuitry would thus not degrade the original optical properties or interfere with the original electronic functions of the APS. The APS could be operated in its normal image-readout

mode or, optionally, it could be operated with the additional circuitry in the brightest-pixel mode. Potential applications could include star tracking or fast tracking of a moving laser-beam spot in laser communication system.

The brightest-pixel mode would be a winner-take-all mode. The pixel intensities would be read out row by row as in ordinary imaging, but unlike in ordinary imaging, the column intensity values for each row would be processed through a winner-take-all circuit (see figure) that would select

the brightest pixel in the row. The intensity reading of the brightest pixel in the row most recently read out would be compared with the previous winner; that is, with the stored intensity reading of the brightest pixel (if any) found in all previous rows. If the greatest intensity reading from the most recent row were greater than the stored intensity reading, then the pixel with this reading would become the new winner, and its intensity reading and coordinates would be stored. Once the intensity readings from all the rows in the APS had been

NASA's Jet Propulsion Laboratory,
Pasadena, California



A Winner-Take-All Circuit would identify the brightest pixel in each row in turn. This pixel would be compared with the brightest pixel found in the preceding rows.

processed in this way, the final winner would be the brightest pixel in the image.

There are several design options for the winner-take-all circuit and the overall mode of operation. In one option, the winner-take-all function would be implemented by a fast current- or voltage-mode analog cir-

cuit. In another option a hybrid analog/digital circuit would generate and compare an increasing voltage (ramp voltage waveform) with intensity-reading voltages for all the columns and would latch the address and intensity value for the column that most recently matched the ramp voltage.

In yet another option, each column pixel in the row read out most recently would be compared with the previous winning pixel in that column and would, if appropriate be declared the new winner. Once the last row had been thus read out and processed, the final column winners would be processed through a winner-take-all circuit to obtain the intensity reading and the address of the brightest pixel in the image. The advantage of this option would be speed, in that the somewhat time-consuming winner-take-all operation would be performed only once per frame period.

This work was done by Orly Yacobi-Pecht, Eric Fossum, and Carver Mead of Caltech for NASA's Jet Propulsion Laboratory. Further information is contained in a TSP (see page 1).

In accordance with Public Law 96-517, the contractor has elected to retain title to this invention. Inquiries concerning rights for its commercial use should be addressed to

Technology Reporting Office

JPL

Mail Stop 122-116

4800 Oak Grove Drive

Pasadena, CA 91109

(818) 354-2240

Refer to NPO-20212, volume and number of this NASA Tech Briefs issue, and the page number.

Monolithic GaAs FET Power Amplifiers for K_a Band

These are prototypes of amplifiers for advanced communication systems.

Lewis Research Center,
Cleveland, Ohio

	Frequency, GHz	Gain, dB	Power, mW	Efficiency, Percent
Initial Program	23.0	15	1.00	25
	29.0	15	0.40	20
	32.5	15	0.25	20
Modification 1	32.5	20	0.10	35
Modification 2	32.5	15	0.25	250
	32.5	10	1.00	235

The Parameters in the Table represent the amplifier-performance goals at various stages of the program.

A program to demonstrate the feasibility of GaAs-based K_a-band power amplifiers has generated a number of technological advances. The goals of the program included (1) capability of amplifier operation at center frequencies of 23, 29, and 32.5 GHz; (2) bandwidth of 5 percent at each center frequency; and

(3) gains and output power levels as specified in the table. Each amplifier was to contain three metal/semiconductor field-effect transistor (MESFET) stages, the MESFET gate width in each stage being larger than that of the preceding stage (see figure). During the program, one- and two-stage amplifier submod-

ules with various input and output network configurations were also constructed and tested to characterize the input, output, and interstage-matching electrical characteristics of the networks.

At the beginning of the program, odd-shaped vapor-phase epitaxial (VPE) MESFET wafers were used. A breakthrough in power and efficiency was achieved by use of lightly doped (doping density $8 \times 10^{17} \text{ cm}^{-3}$) MESFET material grown by molecular-beam epitaxy. At an operating frequency of 34 GHz, a monolithic amplifier that had gate widths of 50, 100, and 250 μm exhibited a gain of 16 dB, yielding an output power of 112 mW with 21.6-percent efficiency.

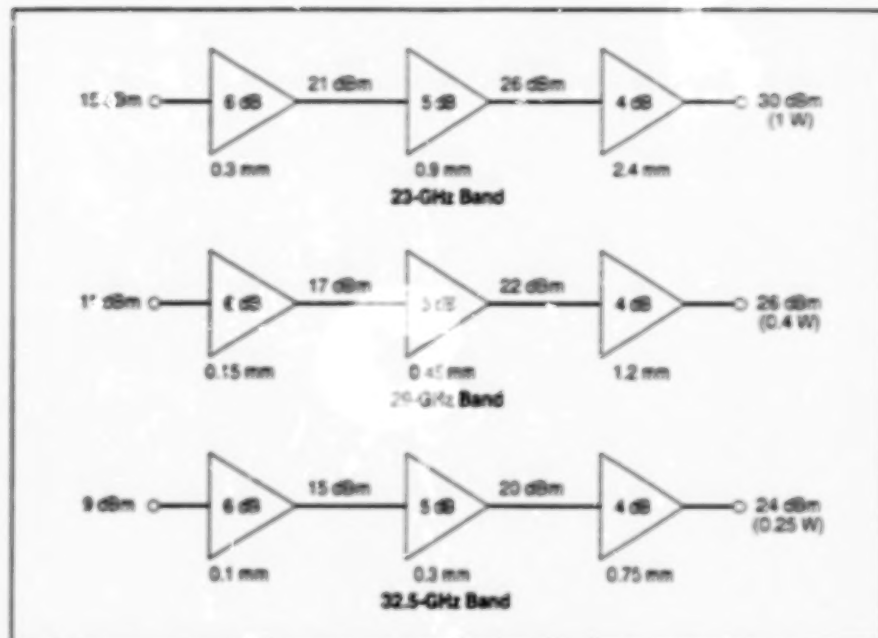
The next breakthrough came with the use of heterostructures grown by MBE (AlGaAs/InGaAs wherein the InGaAs was highly doped). These heterostructures

made it possible to achieve high power density with high efficiency. For example, a single-stage monolithic microwave integrated circuit (MMIC) amplifier containing a MESFET with gate width of 100 μm exhibited an efficiency of 40 percent at 32.5 GHz. The corresponding three-stage amplifier (with gate widths of 50, 100, and 250 μm) put out 180 mW at a gain of 23 dB and an efficiency of 30.3 percent.

The next breakthrough was achieved with 3-in. (7.6-cm) pseudomorphic high-electron-mobility transistor (PHEMT) wafers, each incorporating an etch-stop layer for the gate recess (made by reactive-ion etching). Again, state-of-the-art performances were achieved: efficiency of 40 percent with output power of 235 mW and gain of 20.7 dB. A single-stage $2 \times 600\text{-}\mu\text{m}$ chip generated an output power of 794 mW with a gain of 5 dB and a power-added efficiency of 38.2 percent.

This work was done by Edward J. Haugland of **Lewis Research Center** and Paul Saurier and Hua Quen Tseng of **Texas Instruments, Inc.** Further information is contained in a TSP [see page 1].

Inquiries concerning rights for the



These Block Diagrams depict the basic performance requirements for the amplifier stages. The dimension below each symbol is the MESFET gate width, the decibel number inside each amplifier symbol represents the nominal stage gain, and the other decibel numbers denote nominal power levels at the indicated locations.

commercial use of this invention should be addressed to NASA Lewis Research Center, Commercial Technology Office,

Attn: Tech Brief Patent Status, Mail Stop 7-3, 21000 Brookpark Road, Cleveland, Ohio 44135. Refer to LEW-16626.

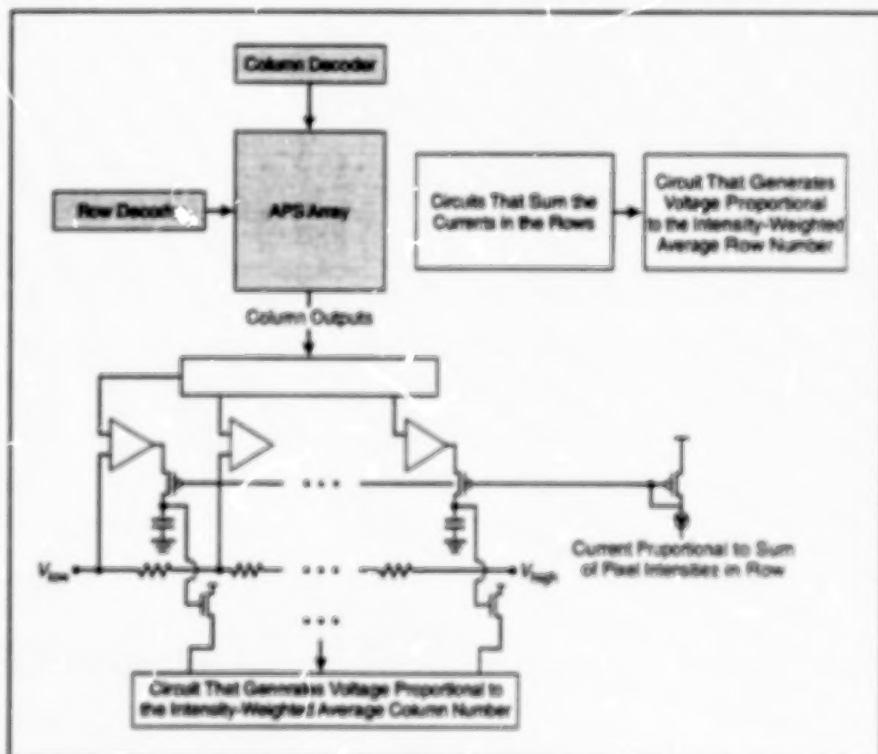
Augmented Active-Pixel Sensors Would Compute Centers of Mass

These sensors could function in either center-of-mass or normal image-readout modes.

NASA's Jet Propulsion Laboratory,
Pasadena, California

Circuits to generate analog or digital representations of the coordinates of the centers of mass of images would be added to imaging photodetector arrays of the active-pixel-sensor (APS) type, according to a proposal. "Centers of mass" as used here is something of a misnomer of historic origin; a more precise term would be "centers of illumination," or, the case of nonlinear or unequal photodetector responses, "centers of response." Regardless of which term one uses, the significance of the proposal is that it would enable APS units to locate and/or track still or moving images representing objects in various states of rest or motion.

For a given APS, the additional circuitry for computing the "center of mass" (COM) would be installed at the periphery of the pre-existing circuitry. The additional circuitry would thus not degrade the original optical properties or interfere with the original electronic functions of the APS. The APS could be operated in its normal image-readout mode, or optionally, it could be operated with the additional circuitry in a COM mode.



Peripheral Circuits would perform COM operations when needed. At other times, the APS array would operate in a normal image-readout mode.

The objective in the COM mode is to generate numbers or analog signals representative of horizontal and vertical pixel coordinates of the center of illumination. In mathematical terms, what one seeks is the brightness-weighted (or response-to-brightness-weighted) average coordinates given by

$$\bar{x} = \frac{\sum_{i=1}^M \sum_{j=1}^N x_j I_{ij}}{\sum_{i=1}^M \sum_{j=1}^N I_{ij}}$$

and

$$\bar{y} = \frac{\sum_{i=1}^M \sum_{j=1}^N y_j I_{ij}}{\sum_{i=1}^M \sum_{j=1}^N I_{ij}}$$

where \bar{x} and \bar{y} are the horizontal and vertical COM coordinates, respectively; x_j is the horizontal coordinate of the j th column; y_i is the vertical coordinate of the i th

row; I_{ij} is the level of illumination (or response to illumination) in the pixel in the i th row and j th column; and M and N are the numbers of rows and columns, respectively.

The COM operation could be implemented by use of analog peripheral circuitry like that shown in simplified form in the figure. Alternatively, the COM operation could be implemented by use of digital peripheral circuitry. Taking one row at a time, the intensity-of-illumination signal from the pixel in each column would be sent to one of the input terminals of a multiplying digital-to-analog converter (MDAC). The column address or other number representative of the horizontal coordinate of the column would be sent to the other input terminal of the MDAC. The product outputs of all the MDACs for all the columns would be summed, then divided by the sum of intensity signals of the columns to obtain the horizontal COM coordinate of the row. Then \bar{x} would be computed as an intensity-weighted aver-

age of the horizontal COM coordinates of all the rows, while \bar{y} would be computed as an intensity-weighted average of the numerical addresses (or other numbers representative of the vertical coordinates) of the rows.

This work was done by Orly Yedid-Pecht, Brad Minch, Bedabrata Pain, and Eric Fossum of Caltech for NASA's Jet Propulsion Laboratory. Further information is contained in a TSP [see page 1].

In accordance with Public Law 96-517, the contractor has elected to retain title to this invention. Inquiries concerning rights for its commercial use should be addressed to

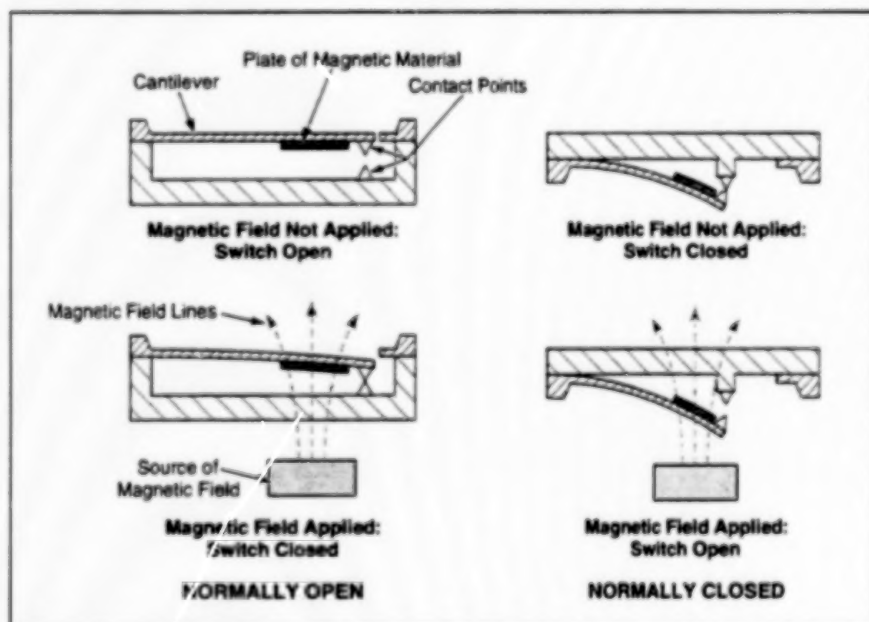
Technology Reporting Office
JPL
Mail Stop 122-116
4800 Oak Grove Drive
Pasadena, CA 91109
(818) 354-2240

Refer to NPO-20210, volume and number of this NASA Tech Briefs issue, and the page number.

Micromachined Magnetostatic Switches

There are numerous potential applications in sensing and control.

NASA's Jet Propulsion Laboratory,
Pasadena, California



A **Micromachined Magnetostatic Switch** operates similarly to a traditional magnetic reed switch, but can be made much smaller.

Magnetostatic switches — switches that open or close in response to magnetic fields — are being developed and fabricated using micromachining (MEMS) technology. These switches operate similarly to traditional magnetic reed switches,

but can be made much smaller. While capable of serving as direct replacements for traditional relays and switches, these MEMS devices open up many new application areas. For example, the magnetostatic switches are being used as

compact, lightweight, energy-efficient replacements for bulky electronic commutation circuitry in brushless dc electric motors. For another example, an array of MEMS switches, each of which opens or closes at a different magnetic-field strength, could serve as a rotary encoder or magnetometer.

The components of a basic micromachined magnetostatic switch are (1) a cantilever-beam spring and supporting structure made of an electrically insulating material, (2) a small plate of magnetic material attached to the cantilever, and (3) contact points and electrical leads made of an electrically conductive material. The switch can be normally open or normally closed. The basic principle of operation is illustrated in the figure. In the presence of a suitably oriented magnetic field, the magnetic force on the soft magnetic plate either bends the cantilever to bring the contacts together (in the case of normally open) or else pulls the contacts apart (in the case of normally closed). When the magnetic field exceeds a threshold value, the switch becomes closed (in the case of normally open) or open (in the case of normally closed).

The large variety of potential designs and materials precludes a complete description in this article. In a typical case, the electrically insulating structural material is oxidized single-crystal silicon. Silicon is chosen both for its attractive mechanical properties and for the potential of integrating the MEMS switches with electronic components in a single monolithic process. A micromachined magnetostatic switch or an array of such switches can be produced on a single silicon wafer or else assembled from two or more substrates. Electromagnet coils can be integrated on the substrate along with the switches to form fully integrated electromagnetic relays.

The soft magnetic material chosen for the prototype micromachined magnetostatic switches is the alloy $\text{Ni}_{80}\text{Fe}_{20}$ (permalloy). High-quality specimens of this

alloy exhibit relative permeability as large as 5,000; this is desirable because the higher the permeability the more sensitive the switch. High-quality films of permalloy can be formed by electroplating.

Gold has been chosen as the electrical-contact material for the prototype switches. Gold can be deposited easily, resists oxidation, and exhibits contact resistances.

Experiments on the prototype switches have yielded some approximate performance figures. Switch contact forces >5 mN, and contact resistances <35 m Ω have been achieved at applied magnetic flux densities of about 0.25 Tesla. Switch lifetimes with hot closures (current flowing immediately upon closure) are in the range of 10^5 to 10^6 cycles at high currents (0.45 A). At low currents (1 mA), switch lifetimes have exceeded 5×10^8 cycles, with no fail-

ures observed.

This work was done by Yu-Chong Tai and John A. Wright of Caltech for **NASA's Jet Propulsion Laboratory**. Further information is contained in a TSP [see page 1].

In accordance with Public Law 96-517, the contractor has elected to retain title to this invention. Inquiries concerning rights for its commercial use should be addressed to

Technology Reporting Office
JPL

Mail Stop 122-116
4800 Oak Grove Drive
Pasadena, CA 91109
(818) 354-2240

Refer to NPO-20415, volume and number of this NASA Tech Briefs issue, and the page number.

BLANK PAGE



Electronic Systems

Hardware, Techniques, and Processes

- 19 Computers for Research on Flight Control in F/A-18 Airplanes
- 19 GPS-Based System Tracks Relative Position of Two Airplanes
- 20 Information-Reduced Carrier Synchronization for Coded PSK Operation at Low-SNR

Books and Reports

- 21 Development of Circuitry for Wristband Radio Transponders

Computers for Research on Flight Control in F/A-18 Airplanes

The cost of testing innovative control laws is expected to be reduced.

Dryden Flight Research Center,
Edwards, California

The Production Support Flight Control Computers (PSFCCs) are flight-control computers that are being developed by NASA in conjunction with the United States Navy. These computers are designed to provide any of the F/A-18 airplanes at NASA Dryden Flight Research Center with capabilities for research in flight-control laws and integrated propulsion/flight-control concepts.

The PSFCCs were conceived to satisfy a need to be able to conduct safe, fast, and efficient flight tests of advanced control laws and handling qualities, on a time-available basis. In the past, design, implementation, and testing of control laws have been extremely expensive and connected directly with specific flight programs under tight schedules. The use of the PSFCCs is intended to reduce the time and cost associated with implementation of new control laws and to enable control-law researchers to spend more time for investigation and discovery in the flight environment.

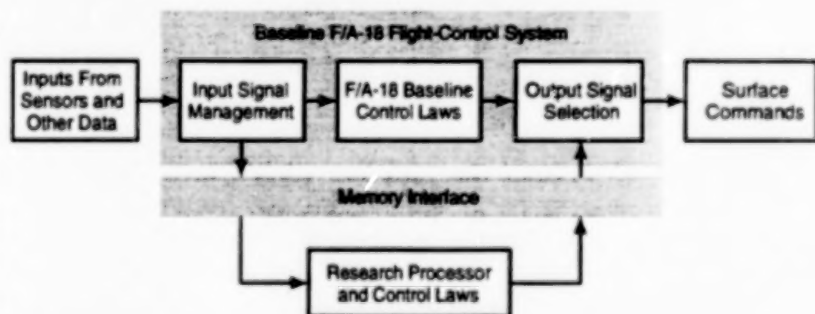
A PSFCC includes a research control-law processor embedded in the flight-control-computer avionics box of an F/A-18 airplane (see figure). The PSFCC enables the pilot to select among research control laws and provides control access to flight-control surfaces and engines. The PSFCC maintains the F/A-18 redundancy-management features and enables immediate return to standard F/A-18 control laws.

The PSFCCs will enable flight testing of new control-law designs with a minimum of system software testing, thereby reducing the time and effort necessary for flight test of new control laws. Because a PSFCC can be installed on any F/A-18 airplane, no dedicated research aircraft is needed; this reduces the schedule and



NASA photo by Carla Thomas

AIRPLANE DURING A TEST FLIGHT



INTEGRATION OF PSFCC INTO BASELINE F/A-18 FLIGHT-CONTROL COMPUTERS

A PSFCC is integrated into a baseline F/A-18 flight-control system. A PSFCC can be installed in any F/A-18 airplane that happens to be available for a flight test.

programmatic pressures on control-law researchers.

At present, the PSFCCs have gone through initial flight test and are being prepared for initial experiments involving alternate control sticks, flexible-wing parameter

identification, and aircraft formation flight.

This work was done by John Carter of Dryden Flight Research Center. Further information is contained in a TSP [see page 1].
DRC-98-78

GPS-Based System Tracks Relative Position of Two Airplanes

Data from this system will be used to control precise maneuvers for schlieren photography.

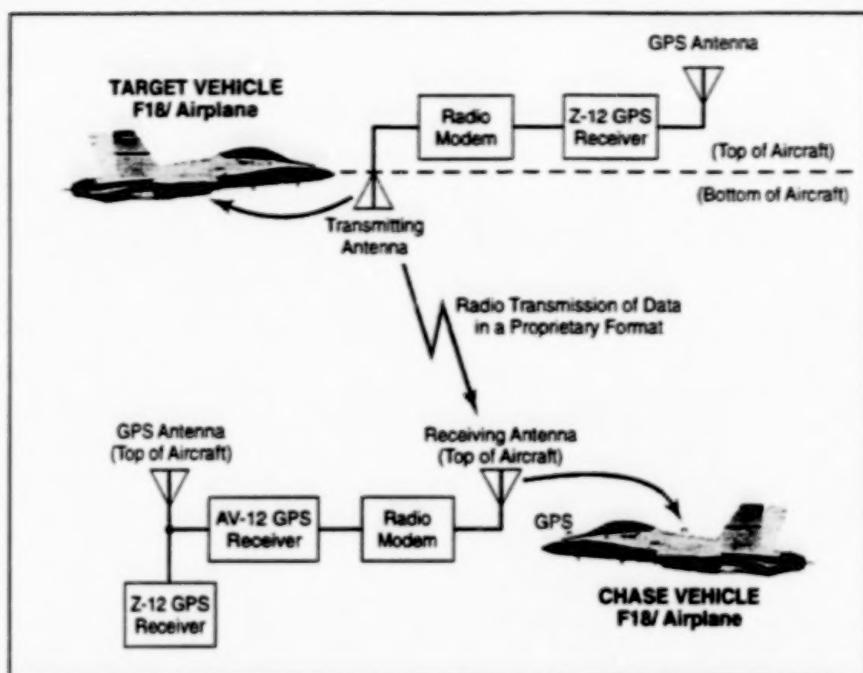
Dryden Flight Research Center,
Edwards, California

A developmental electronic system that includes Global Positioning System (GPS) receivers is designed to track the relative position and velocity to two airplanes in real time. In the original application for which the system is being developed, one F-18 airplane (denoted the "chase vehicle") is to be used to take schlieren photographs of shock waves generated by the another F-

18 airplane (denoted the "target vehicle"). When fully developed, the system would afford the precise position and time measurements needed to accomplish the schlieren shock-wave photography.

The system includes two GPS receivers (of types called "AV-12" and "Z-12") connected to the same antenna in the chase vehicle, and a single Z-12 GPS receiver in

the target vehicle. Special-purpose software in the AV-12 receiver in the chase vehicle determines the absolute position of the chase vehicle by use of data received via the L1 [coarse-acquisition (C/A) GPS Code]. Before the relative position and velocity can be determined, the AV-12 receiver in the chase vehicle must receive GPS data from the Z-12 GPS receiver in



A GPS-Based System comprising subsystems in both airplanes provides data on their relative position and velocity.

the target vehicle. These data are transmitted to the chase vehicle as part of a message in a proprietary format. The relative-position and relative-velocity data can be used three ways: (1) viewed in real time on a display on the AV-12 receiver, (2) passed on to other computers, and (3) stored for later evaluation.

Previous tests of the system were performed on the ground. Flight tests now under way involve the following operations:

- Simultaneously with the operation of

the GPS receivers in the chase vehicle, the Z-12 receiver in the target vehicle logs its own position data. These data are downloaded to a laptop computer after a flight test for post-processing correction.

- The output data from the AV-12 receiver in the chase vehicle are saved in the aircraft data recording system. The data from the Z-12 receiver in the chase vehicle are taken to indicate the position of the chase vehicle and are logged inter-

nally. A laptop computer is used to download the data from this Z-12 receiver after a flight test, also for post-processing correction.

Preliminary results of the flight tests include observations of unexpected dropouts in the relative-position calculations. This observation indicates a need for tests to verify the quality of the communication lines between the transmitting and receiving antennas and the radio modems.

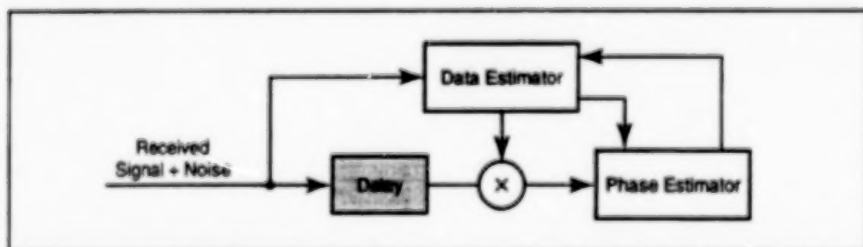
When dropouts do not occur, the accuracy achieved in flight tests is characterized by lateral position errors within ± 3 m and vertical position errors within ± 4 m with 2-m bias. This level of accuracy is more than adequate for schlieren photography between aircraft using the Sun as the light source. In planned flight tests, the data generated by the developmental system will be used, during subsonic flight of the chase vehicle and supersonic flight of the target vehicle, to momentarily position the chase vehicle to eclipse the Sun as viewed from the target vehicle. The data will also be used to trigger the photograph at the precise time of the artificial eclipse thus produced. The goal is to make detailed photographs of shock waves about the target vehicle.

This work was done by Edward A. Haering, Jr., and Glenn Bever of Dryden Flight Research Center and Joe Collura of TYBRIN Corp. Further information is contained in a TSP [see page 1].
DRC-98-80

Information-Reduced Carrier Synchronization for Coded PSK Operation at Low-SNR

Symbol (and thus phase) estimates are improved iteratively.

NASA's Jet Propulsion Laboratory,
Pasadena, California



The Proposed Information-Reduced Carrier-Synchronization System would effect an iterative process in which data estimates would result in improved phase estimates which would result in improved data estimates, and so on. Theoretical calculations have shown that in comparison with other carrier-synchronization systems for coded BPSK, this system would offer superior tracking performance.

An information-reduced carrier-synchronization (IRCS) system has been proposed for use in a coded binary-phase-shift-keying (BPSK) radio-communication receiver

subject to a low signal-to-noise ratio (SNR). The term "information-reduced" alludes to the use of an estimate of the instantaneous data symbol (and thus of the instantaneous

phase modulation) to reduce the amount of randomness (and thus the amount of information) in the signal being processed in the carrier synchronizer.

In IRCS, the reduction of the amount of information is effected by attempting to convert the received modulated carrier to an unmodulated carrier (pure tone) before applying it to a phase-tracking loop, in the hope of improving performance. Traditional IRCS systems for synchronization with carrier signals modulated by BPSK include Costas loops, data-aided loops, and demodulation/remodulation loops. The traditional systems are designed to implement various approximations of a closed-loop structure that effects maximum a posteriori (MAP) estimation of

phase. The degradation of tracking performance of such a loop in the case of BPSK is represented by a quantity called the "squaring loss," which is a measure of the degradation of the receiver signal-to-noise ratio and is associated with the mean-squared phase error of the loop. In the case of a conventional in-phase/quadrature (I-Q) carrier-tracking loop, the mean-square phase error is a result of signal and noise cross products that are generated in the effort to remove the data modulation from the loop error signal. At low symbol SNR, the squaring loss of an I-Q loop can be severe enough to prevent tracking.

If the data sequence and its timing were completely known, then a BPSK signal could be converted to a pure tone simply by multiplying the BPSK signal by the data waveform. One could then track the unmodulated carrier with improved performance by use of a phase-locked loop, which does not exhibit squaring loss.

Short of complete knowledge of the data waveform and in the presence of noise, the best approximation of a pure tone could be obtained by feeding back an estimate of the data waveform corresponding to tentative decisions on the data symbols. Such feedback is called "decision feedback" for short.

Decision feedback is used within the traditional loops, but is not used to modify the loop structures. In the proposed IRCS system (see figure), decision feedback would be introduced at the input terminal of the loop; simultaneously, the structure of the loop would be modified (in the sense that its parameters would be modified) on the basis of the associated change in data-transition statistics in the input. The transition probability would be reduced from 1/2 (characteristic of BPSK signals in the absence of feedback) to a value closer to zero, so that the input signal would be converted to a close approximation of

a pure tone, with a resultant improvement in carrier-tracking performance over conventional I-Q loops.

Although initially available data-waveform estimates are generally of low quality, they can be used to initiate the IRCS process by reducing the number of data transitions at the input. Once phase lock was achieved, the improved phase estimates could be fed back to the data detector, yielding improved symbol estimates for feedback, and thereby achieving even better phase tracking. This iterative process could eventually lead to virtual elimination of squaring loss, so that the performance of the system would approach that of a phase-locked loop operating on an unmodulated carrier signal.

This work was done by Victor Vinnrotter and Marvin Simon of Caltech for NASA's Jet Propulsion Laboratory. Further information is contained in a TSP [see page 1]. NPO-20261

Books and Reports

Development of Circuitry for Wristband Radio Transponders

A document proposes the development of several alternative types of electronic circuits for wristband transponders for the system described in "Person-Locator System Based on Wristband Radio Transponders" (NPO-19280) NASA Tech Briefs, Vol. 19, No. 12 (December 1995), page 40. To recapitulate: microscopic transponder circuits embedded in wristbands would be powered by modulated signals radiated by transceiver nodes and would respond by transmitting signals modulated with unique digital codes to identify the wearers. Circuits of the first proposed type would operate in a conventional voltage mode (meaning that

signal levels would be defined primarily in terms of potentials); these circuits would be designed and fabricated by use of multichip-module or hybrid-circuit technology; a subtype would be designed and fabricated by use of complementary metal oxide/semiconductor (CMOS) technology. The circuits of the second type would be of the CMOS variety and would function in a current mode (signal levels would be defined primarily in terms of currents). The document includes a brief discussion of the advantages of the current mode in the proposed application; these advantages include superior high-frequency performance and independent control of closed-loop gain and bandwidth.

This work was done by Victor Boyadzhyan and Frederick Mintz of Caltech for NASA's Jet Propulsion

Laboratory. To obtain a copy of the document, "Passive RF Transponder and Other RF Circuitry Implemented by Current Mode Enabling Technology," see TSP's [page 1].

In accordance with Public Law 96-517, the contractor has elected to retain title to this invention. Inquiries concerning rights for its commercial use should be addressed to

Technology Reporting Office

JPL

Mail Stop 122-116

4800 Oak Grove Drive

Pasadena, CA 91109

(818) 354-2240

Refer to NPO-20100, volume and number of this NASA Tech Briefs issue, and the page number.

BLANK PAGE



Physical Sciences

Hardware, Techniques, and Processes

- 25 Microfabricated Ice Sensors
- 26 Methanol-Fuel-Cell Bipolar Plate Improved for Removal of Water

Books and Reports

- 26 Study of DLS Monitoring of the Growth of Protein Crystals

BLANK PAGE

Microfabricated Ice Sensors

Presence of ice is inferred from stiffening of a capacitive actuator/sensor.

Lewis Research Center,
Cleveland, Ohio

Microfabricated, silicon-based capacitive actuator/sensor devices have been developed as prototypes of compact, low-power transducers that would be used to detect the presence (and perhaps eventually measure the thickness) of ice on aircraft lift and control surfaces. These transducers would be mounted flush with surfaces, so that they would not perturb airflows. Transducers of this type could also be used in such diverse applications as detecting ice in refrigerators for triggering defrosting cycles and detecting ice on roadways to trigger warning signals for drivers.

Figure 1 presents a simplified cross-sectional view to illustrate the basic device configuration and ice-detection principle. The main supporting structure is a low-thermal-expansion glass wafer containing a rectangular hole 1 to 3 mm on a side and about 2 to 3 μm deep on its upper surface. The glass wafer is capped by a 7- μm -thick silicon wafer that has been heavily doped with boron to make it highly electrically conductive. The part of the wafer over the hole constitutes both a diaphragm and one electrode of a three-electrode parallel-plate capacitor. The other two capacitor electrodes are concentric rectangular patches of aluminum, about 0.3 μm -thick, on the bottom of the hole; the inner patch serves as the driving electrode, while the outer one serves as the sensing electrode, as explained below. Vent holes (not shown in the figure) between the hole and the outside prevent spurious deflection of the diaphragm by changes in ambient air pressure.

In use, the upper (outer) surface of the diaphragm and the rest of the doped silicon wafer is mounted flush with an aircraft or other surface of interest. A dc potential is applied between the driving electrode and the diaphragm to deflect the diaphragm slightly into the hole by electrostatic attraction. The amount of deflection is inferred from the change in capacitance between the diaphragm and the sensing unit; for this purpose, the diaphragm and sensing electrode are connected as the terminals of an input capacitor in a frequency-modulation circuit with a nominal frequency of 48 MHz, and the change in capacitance is determined from the change in frequency.

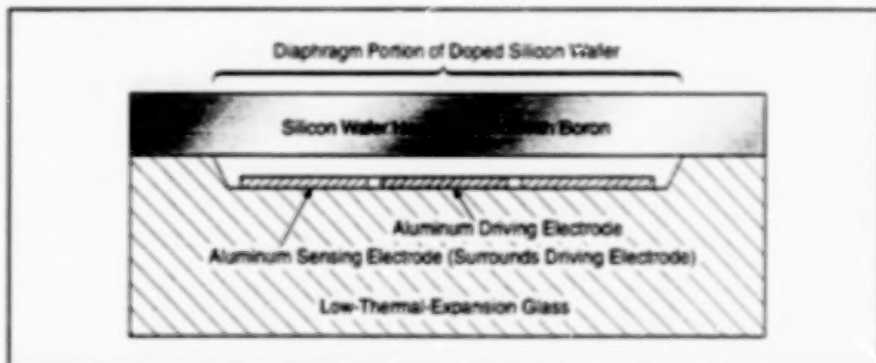


Figure 1. This Microfabricated Actuator/Sensor Device is used to detect ice on the upper (outer) diaphragm surface. The diaphragm is deflected electrostatically by application of voltage to the driving electrode. The amount of deflection (which decreases in the presence of ice) is measured capacitively via the sensing electrode.

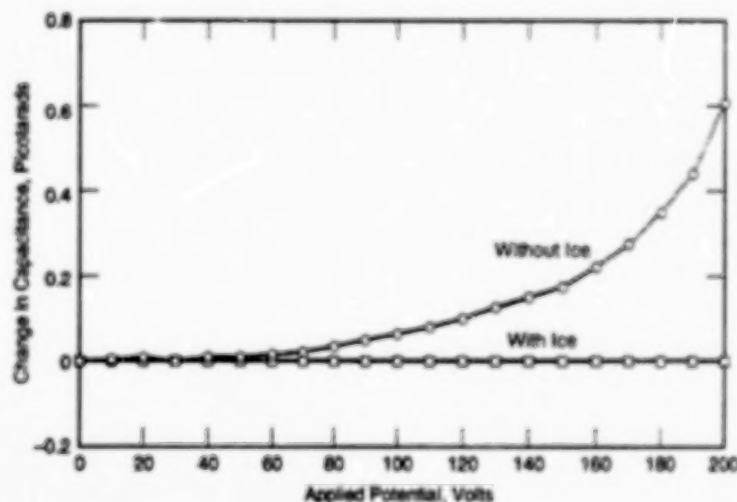


Figure 2. The Change in Capacitance as a function of driving voltage was measured in an experiment on a prototype device, with and without ice on the outer surface. In this device, the diaphragm was square, 1 mm on a side.

A deposit of ice on the outer diaphragm surface stiffens the diaphragm, reducing the deflection and thus the change in capacitance for a given driving voltage (see Figure 2). The presence of ice can thus be inferred from the reduction in the change in capacitance for a given applied potential.

Future versions of these devices may afford the capability to determine the thickness of ice according to the following principle: The diaphragm would be designed to vibrate at a suitable resonance frequency. In operation, the resonance would be excited and its frequency measured, and the thickness of ice would be determined

from any deviation from a nominal (no-ice) resonance frequency.

This work was done by Russell G. DeAnna of the U. S. Army Research Laboratory and Mehran Mehregany and Shuvo Roy of Case Western Reserve University for Lewis Research Center. Further information is contained in a TSP [see page 1].

Inquiries concerning rights for the commercial use of this invention should be addressed to NASA Lewis Research Center, Commercial Technology Office, Attn: Tech Brief Patent Status, Mail Stop 7-3, 21000 Brookpark Road, Cleveland, Ohio 44135. Refer to LEW-16633.

Methanol-Fuel-Cell Bipate Improved for Removal of Water

Low-pressure airflow from an ordinary fan is sufficient.

NASA's Jet Propulsion Laboratory,
Pasadena, California

An improved design for a bipate in a methanol fuel cell provides increased efficiency in the removal of water, relative to older designs. For reasons explained below, this design both improves the performance of the fuel cell and increases the overall energy efficiency of the power-generating system of which the fuel cell is a part.

A typical methanol fuel cell includes a number of membrane/electrode assemblies (MEAs) stacked in alternation with bipates. Each bipate serves partly as an electrical contact between the cathode of the MEA on one side and the anode of the MEA on the other side. The bipate also contains channels for circulating air past the cathode and other channels for delivering fuel (methanol) to the anode.

During operation of the fuel cell, several parasitic chemical and physical effects cause water to accumulate in the air channels. If the water is not removed, then it impedes airflow in the channels, and consequently, the fuel-cell performance deteriorates. In the cases of most older bipate designs, considerable power is expended to supply pressurized air to blow the water out of the air channels; as a result, overall energy efficiency is reduced. The energy-efficiency issue becomes even more important if the fuel cell is operated at room temperature (about 25 °C, in contrast to a typical higher operating temperature of about 95 °C) because the fuel-cell output decreases with decreasing temperature in this range.

The improved bipate is designed to exploit gravitation and surface tension to remove water without need to supply pressurized air. It is still necessary to bring in air for the electrochemical reaction in the fuel cell, but the improved bipate offers little resistance to airflow, so that a low-power fan that supplies air at slightly more than atmospheric pressure is sufficient. Thus, a high level of performance can be maintained, and energy efficiency is enhanced.

To enable gravitation to drain water from the fuel cell, the airflow channels in the improved bipate are oriented vertically, with inlets at the top and outlets at the bottom (see figure). Most of the bipate is made of a graphite/epoxy composite material, which is hydrophobic. Unfortunately, hydrophobic surfaces tend to impede drainage. Therefore, the drainage surfaces of the bipate are treated to make them hydrophilic, so that immediately upon release at the cathode, a drop of water becomes part of a surface layer of water that drains to the bottom of the bipate. The treatment to make the surfaces hydrophilic includes coating with a commercial perfluorosulfonic acid-based ion-exchange polymer followed by coating with a carbon-supported platinum/ruthenium catalyst. The combination of coating materials was chosen because it is chemically compatible with other fuel-cell materials and is expected to be chemically stable in the long term.

If nothing were done to prevent it, sur-

face-tension effects could cause an air-outlet port at the bottom of the bipate to become plugged with water. Two features prevent this from happening: (1) the port is made large enough that water cannot straddle it and (2) a metal insert extending from the edge of the bipate wicks the water away from the port. At the edge of the insert, water forms into drops, which then fall off.

To minimize resistance to airflow, air is supplied to the bipate via a large external manifold. The air passes from the manifold into the bipate through a large inlet port (equal in size to the outlet port). The air channels in the bipate are also made large to minimize resistance to flow.

This work was done by Andrew Kinder and Albany Lee of Caltech for NASA's Jet Propulsion Laboratory. Further information is contained in a TSP (see page 1).

In accordance with Public Law 96-517, the contractor has elected to retain title to this invention. Inquiries concerning rights for its commercial use should be addressed to

Technology Reporting Office

JPL

Mail Stop 122-116

4800 Oak Grove Drive

Pasadena, CA 91109

(818) 354-2240

Refer to NPO-20308, volume and number of this NASA Tech Briefs issue, and the page number.

Books and Reports

Study of DLS Monitoring of the Growth of Protein Crystals

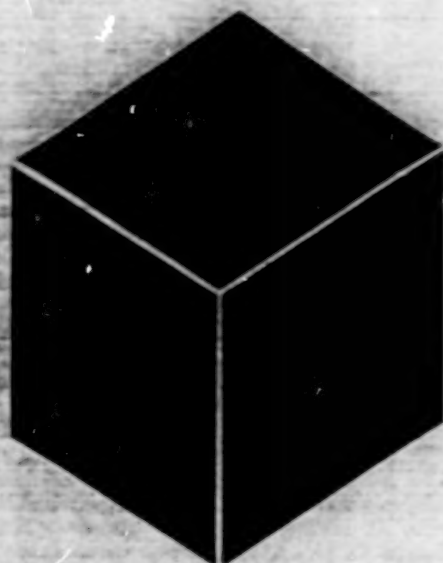
A report describes an experimental study of whether an advanced fiber-optic dynamic light-scattering (DLS) probe affords the capability for noncontact detection of particles of various sizes associated with the stages of growth of protein crystals in automated hanging-drop protein-growth apparatuses. [A related previous report was described in "DLS Sizing of Particles in Hanging Liquid Drops" (LEW-16515), NASA Tech Briefs, Vol. 21, No. 12 (December 1997), page 98.] The DLS probe used in this study was a modified

version of the one described in "Compact, Noncontact Fiber-Optic Probe for Diagnosis of Eye Diseases" (LEW-16429), NASA Tech Briefs, Vol. 22, No. 2 (February 1998), page 82, and was augmented with a miniature microscope for viewing protein crystals. In the experiments, the probe was found to yield data on the distributions of particle sizes at various times (with a potential temporal resolution of a few seconds) during the operation of three different protein-growth apparatuses. It was concluded that the probe affords the desired capability and may therefore eventually contribute to understanding of the processes involved in crystallization of proteins.

This work was done by Rafiq R. Ansari of Case Western Reserve University; Kwang I.

Suh of the National Research Council; Lawrence J. DeLucas, Alireza Arabshahi, and Terry L. Bray of the University of Alabama at Birmingham; and W. William Wilson of Mississippi State University for Lewis Research Center. To obtain a copy of the report, "A Fiber Optic Probe for Monitoring Protein Aggregation, Nucleation, and Crystallization," see TSP's [page 1].

Inquiries concerning rights for the commercial use of this invention should be addressed to NASA Lewis Research Center, Commercial Technology Office, Attn: Tech Brief Patent Status, Mail Stop 7-3, 21000 Brookpark Road, Cleveland, Ohio 44135. Refer to LEW-16611.



Materials

Hardware, Techniques, and Processes

- | | |
|----|--|
| 29 | Versatile Transparent-Melt Crystal-Growth Systems for Organic Nonlinear Optical Materials Using Bridgman-Stockbarger Technique |
| 30 | Vapor Drying for Preparing InGaAsP for Epitaxial Regrowth |
| 31 | Improved Process for Scrubbing and Treating NO _x Liquor |
| 32 | Rapid Densification of Ceramic Monoliths and Composites |

BLANK PAGE

Versatile Transparent-Melt Crystal-Growth Systems for Organic Nonlinear Optical Materials Using Bridgman-Stockbarger Technique

New crystallization technique allows for viewing and temperature changes.

Marshall Space Flight Center,
Alabama

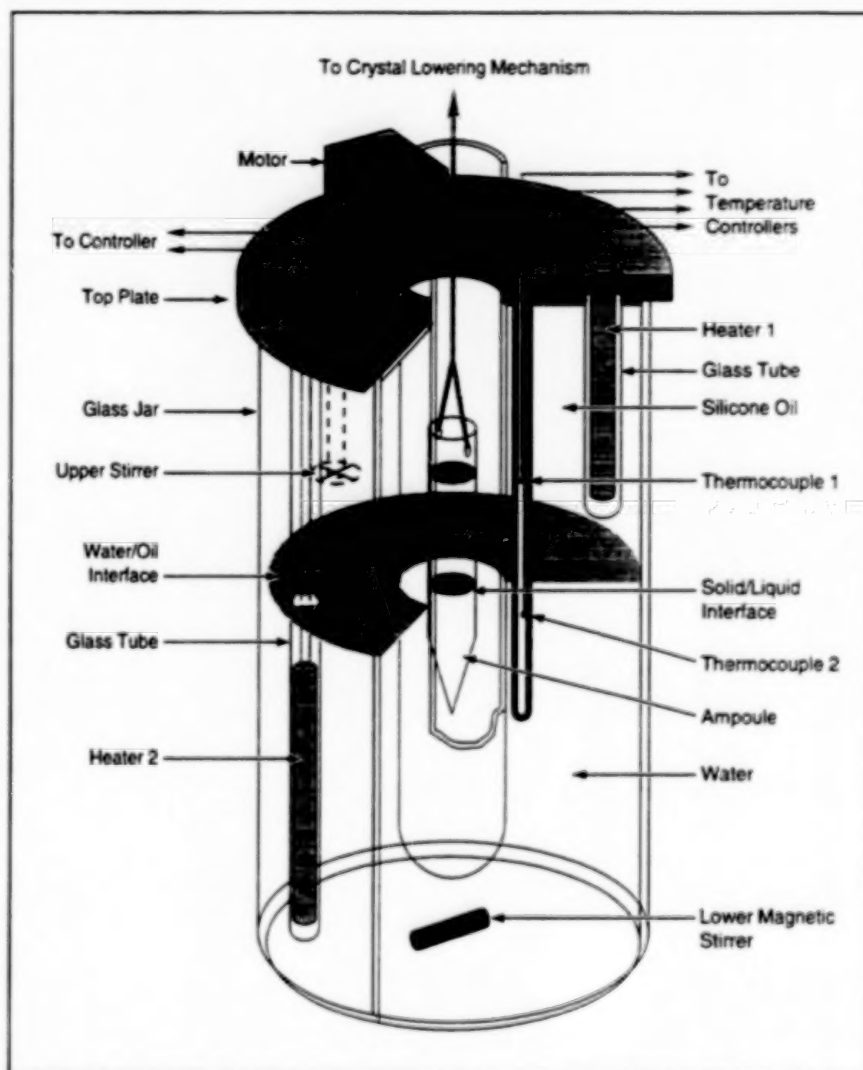
Single crystals of benzil, benzil aniline, and salicylidene-aniline have been successfully grown using a modified Bridgman-Stockbarger technique for three different crystal-growth systems. The unique feature of the Bridgman-Stockbarger technique is that the crystal-melt surface can be viewed from any direction, and the temperature between the hot and cold zones can be adjusted at any time during the melt.

First, scientists at NASA's Marshall Space Flight Center in Huntsville, Alabama, and Alabama A & M University, Normal, Alabama, designed and fabricated the melt-growth system using two immiscible liquids. In this crystal-growth system, two zones were made up of immiscible liquids, water, and silicone oil. These two liquids were contained in a right circular glass cylinder. Each zone was individually heated and stirred for temperature uniformity within the zone, and the temperature of each zone was controlled by a PID controller to within $\pm 0.1^\circ\text{C}$.

The organic material was placed in a clean glass ampoule and lowered slowly from the hotter zone to the cooler zone. Lowering speeds of less than 0.2 millimeters per hour were required to grow good-quality crystals. This system was limited to temperatures of 85°C or less since one of the zones contained water. Crystals of nonlinear optical material salicylidene-aniline were grown using this system.

To extend the temperature range, a second system was constructed using aluminum end plates and glass walls to contain the heated fluids. Glass cylinders 4 in. (10 cm) in diameter were cut and polished at both ends. An O-ring groove was cut into each end plate and filled with a silicone two-part adhesive. Two separate zones were stacked, one on top of the other. The temperature of each zone was controlled separately by circulating constant-temperature silicone oil using Neslab high-temperature circulating baths.

Also, in this crystal-growth system, a glass conical-tip ampoule was used as a crucible. A conventional crystal-pulling-and-rotation system was used to lower the ampoule through the zones.



The Bridgman-Stockbarger melt-growth system uses two immiscible liquids.

Over the last three years, a variety of organic nonlinear crystals have been grown using this melt-growth system.

Finally, an all-glass melt-growth system was used for larger diameter bulk single crystals. To alleviate the problem of clear visualization of the growth interface, an all-glass melt-growth system was designed and fabricated in Alabama A & M University's glass-blowing shop.

This system again uses a two-zone system, but was constructed to allow for the growth of larger diameter (25 mm) organic crystals. The temperature was controlled by Neslab constant-temperature

baths by circulating silicone oil. A commercial crystal-pulling system was used to lower the ampoule through the zones.

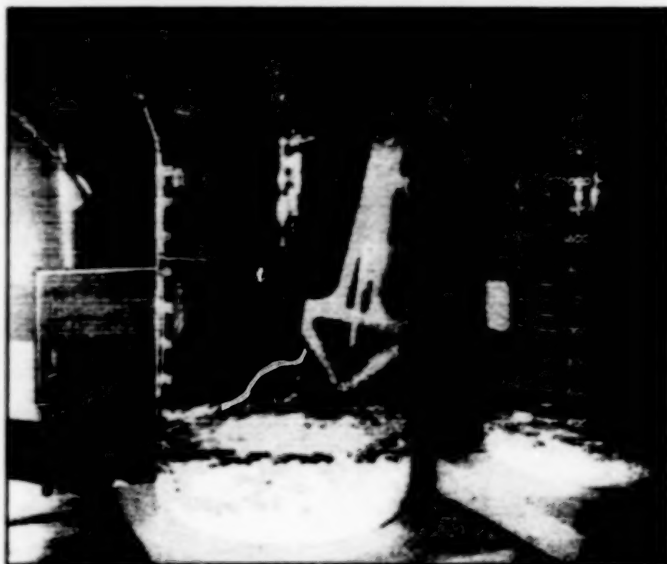
This work was done by M.D. Aggarwal, W.S. Wang, J. Choi, and Robert Metz of Alabama A & M University of Normal, Alabama, and Benjamin G. Penn and Donald O. Frazier of Marshall Space Flight Center. Further information is contained in a TSP [see page 1].

Inquiries concerning rights for the commercial use of this invention should be addressed to the Pattnel, Marshall Space Flight Center [see page 1]. Refer to MFS-26439.

Vapor Drying for Preparing InGaAsP for Epitaxial Regrowth

Traces of water and other contaminants are removed in a three-step treatment.

NASA's Jet Propulsion Laboratory,
Pasadena, California



A Simple Vapor Degreasing Still can be made with a 2,000-mL beaker of Pyrex (or equivalent) low-thermal-expansion glass. The bottom of the beaker is covered with polytetrafluoroethylene boiling stones, 600 mL of an organic solvent is brought to a boil, and a cover glass is placed over the top. The substrate to be treated is mounted on a polytetrafluoroethylene holder and lowered into the vapor space through a slit in the cover glass.

A vapor drying treatment removes traces of water and other contaminant residues that remain on the surface of a patterned semiconductor substrate after chemical cleaning in preparation for subsequent epitaxial growth on the substrate. The treatment was developed in conjunction with attempts at epitaxial regrowth of first-order gratings for distributed-feedback lasers in the InGaAsP material system.

A chemical cleaning typically ends with a rinse in deionized water followed by drying in isopropyl alcohol vapor followed by blow drying with nitrogen. Notwithstanding the apparent thoroughness of the drying steps, the amount of water and other contaminants that remain on the cleaned surface is sufficient to give rise to a large number of defects in epitaxial material.

The present vapor drying treatment is essentially a modified, three-step vapor degreasing procedure. It was selected from among a number of similar treatments in experiments based on the conjecture that aggressive vapor degreasing might be capable of removing water vapor that sticks to the surface of a substrate after cleaning and conventional drying. In each step of the treatment,

the substrate is lowered into a still filled with a solvent vapor (see figure) and kept there for a few minutes.

Of a number of different combinations of vapor dips that were tested in the experiments, the one that proved most successful in removing water vapor from the surface of a cleaned substrate was acetone followed by trichloroethylene followed again by acetone. The trichloroethylene in this combination was initially chosen with the expectation that it would remove any organic residue that would assist in keeping water vapor on the surface. However, since water does not dissolve easily in trichloroethylene, an initial dip in acetone vapor was added to remove as much water vapor as possible from the surface before immersion in trichloroethylene vapor. Furthermore, since acetone easily mixes with trichloroethylene and is more volatile, acetone was also chosen for the final vapor dip, not only to remove trichloroethylene from the surface but also to leave a thin surface layer of solvent that would either quickly evaporate upon removal from the vapor bath, or else would be quickly desorbed upon heating of the substrate to growth temperature.

BEFORE TREATMENT

Element	Atomic Percent
As	11.01
Ga	2.14
C	45.21
In	9.57
O	32.08

AFTER TREATMENT

Element	Atomic Percent
As	23.79
Ga	4.50
P	11.66
C	20.14
In	18.41
O	21.49

The Composition of the Surface of an InGaAsP substrate was determined by XPS before and after the treatment described in the text. The treatment caused a reduction in the carbon and oxygen contents and the appearance of phosphorus — all indications of a very clean surface.

In the experiment on this treatment, a specimen substrate was first dipped in acetone vapor for 5 minutes to ensure removal of water vapor. Condensation — most likely acetone — was observed on the substrate and substrate holder throughout this step of the treatment. Next, the substrate was placed in trichloroethylene vapor for 5 minutes. Once again, condensation — most likely trichloroethylene — was observed on the substrate. Finally, the substrate was again exposed to acetone vapor to remove the trichloroethylene from its surface and saturate the surface with the more volatile acetone. The substrate was left in the acetone vapor for 5 minutes. Surprisingly, about two minutes into this last step, all noticeable drops of condensation vanished from the substrate and substrate holder, leaving behind extremely dry surfaces.

The precise physical mechanisms responsible for the effectiveness of this three-step vapor drying treatment remain unknown. What is known is that the technique is so effective in drying the surface as to prevent most of the defects that would otherwise form in epitaxially deposited material. Moreover, analysis of a substrate by x-ray photoelectron spectroscopy (XPS) reveals that the three-step treatment reduces the amount of carbon and oxygen contaminating the surface (see table). The remaining carbon and oxygen have been

tentatively attributed to exposure of the substrate to air during transfer to the XPS apparatus.

This work was done by James Singletery, Jr., of Caltech for NASA's Jet Propulsion Laboratory. Further information is contained in a TSP [see page 1].

In accordance with Public Law 96-517, the contractor has elected to retain title to this invention. Inquiries concerning rights for its commercial use should be addressed to

Technology Reporting Office
JPL

Mail Stop 122-116
4800 Oak Grove Drive
Pasadena, CA 91109
(818) 354-2240

Refer to 19899, volume and number of this NASA Tech Briefs issue, and the page number.

Improved Process for Scrubbing and Treating NO_x Liquor

The pH and H₂O₂ are controlled to produce potassium nitrate fertilizer while scrubbing.

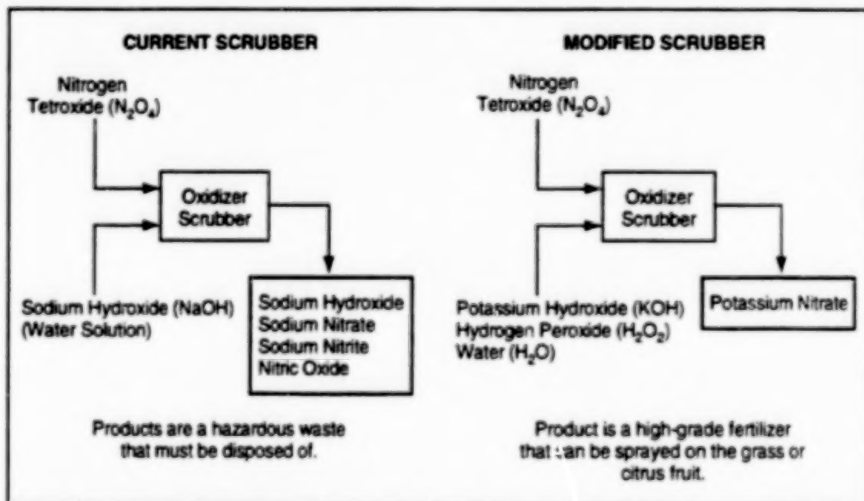
John F. Kennedy Space Center,
Florida

A new process and equipment have been developed for reducing the emissions of hazardous nitrogen oxides (NO_x), and eliminating a hazardous waste stream. In this process, a waste gas stream of nitrogen and NO_x, arising from spacecraft-propellant operations, is reacted (scrubbed) with a dilute solution of hydrogen peroxide (scrubber liquor). The resulting liquor is treated simultaneously with potassium hydroxide during the scrubbing operation to produce potassium nitrate. The overall effect of the process is to absorb NO_x from the waste gas stream into the scrubber liquor where NO_x is converted into an aqueous solution of potassium nitrate, which can be used as a fertilizer.

In the original application for which the process and equipment were developed, NO_x is an undesired gaseous effluent from the handling of nitrogen tetroxide, a hypergolic propellant oxidizer used in space shuttle and Titan rockets. The process and equipment could also be adapted to removal of NO_x from flue gases, ventilation streams from metal-pickling operations, and other gaseous effluent streams.

As in a typical scrubber process, the improved process has a scrubber liquor pumped to the top of a tower and sprayed down through packing, while the gaseous mixture rises through the column and is vented after being scrubbed by the falling liquor. The concentration of hydrogen peroxide (H₂O₂) is controlled to 1.0 percent in the liquor storage tank by automatic addition of 35-percent H₂O₂. Also, the pH is maintained at 7.0 by the automatic addition of potassium hydroxide solution.

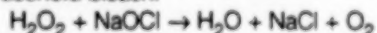
Scrubber liquor is continually sampled during scrubbing to determine the pH and hydrogen peroxide concentration. A commercial controller monitors pH and adds 45-percent potassium hydroxide



A Comparison of the current oxidizer scrubber process with the new proposed scrubber process shows the advantage of the modified configuration.

solution, as needed. The potassium hydroxide reacts with nitric acid produced in the liquor, as nitrogen tetroxide is scrubbed. As the liquor is recycled back to absorb more oxidizer, the concentration of potassium nitrate builds up to a maximum of 15 weight percent, after which it is stored in a separate tank for shipment to fertilizer use areas.

A new invention, the NO_x control system including the hydrogen peroxide controller, repeatedly takes small samples of the scrubber liquor and measures the peroxide content. A programmable logic controller activates switches, valves, and pumps to control the rate of addition of a 35-percent hydrogen peroxide solution to maintain a 1-percent peroxide concentration in the bulk liquor. The hydrogen peroxide controller (see figure) is based on the chemical reaction between hydrogen peroxide and sodium hypochlorite, ordinary household bleach:



This reaction takes place in a closed vessel, so that the increase in pressure

from generation of O₂ can be measured as an indication of the amount of H₂O₂ in the sampled scrubber liquor.

The improved process is intended to replace an existing process in which the scrubber liquor is a 25-weight-percent solution of sodium hydroxide. When all impacts of both processes are considered, the improved process is found to cost less, to eliminate a hazardous waste stream, to lower NO_x emissions, and to produce a valuable liquid fertilizer instead.

This work was done by Dale E. Lueck of Kennedy Space Center and Clyde F. Parrish and Ronald G. Barile formerly of I-Net. Further information is contained in a TSP [see page 1].

This invention is owned by NASA, and a patent application has been filed. Inquiries concerning nonexclusive or exclusive license for its commercial development should be addressed to the Patent Counsel, Kennedy Space Center; (407) 867-6225. Refer to KSC-11884.

Rapid Densification of Ceramic Monoliths and Composites

New technology enables rapid, low-cost manufacturing of partially-dense and fully-dense devices and components of ceramic compositions.

Marshall Space Flight Center,
Alabama

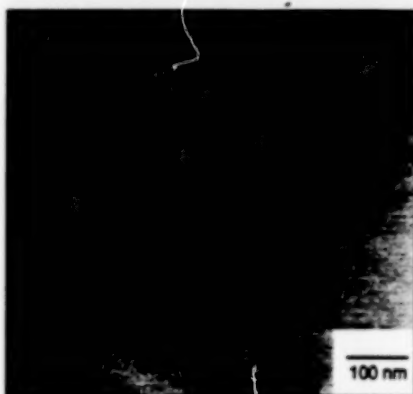
A rapid densification technology uses nanostructured powders to produce ceramic devices and components. This technology provides ceramic monoliths and composites that can be used in the automobile, energy, electrochemical, magnetic, structural, biomedical, computing, information-transfer, and pollution-prevention-and-control industries.

Nanoscale powders of ceramic, measuring less than 100 nm, were mixed with less than 5 weight percent of sintering aid, cold pressed into pellets, and pressureless sintered between 1,400 and 1,600 °C. The sintering environment was evacuated to remove oxygen and maintained in evacuated reducing state.

Micron-scale powders of ceramics with the same composition were also processed through the same steps under similar environments.

The densification of a ceramic compact, or sintering, is the process of removing the pores between the starting particles combined with growth and strong bonding between adjacent particles. The driving force for densification is the decrease in surface area and lowering of the surface free energy by the elimination of the solid-vapor interface.

Nanostructured powders are a novel class of materials whose distinguishing feature is that their average grain or other structural domain sizes are below 100 nm. Within this size range, a variety of confinement effects significantly change the properties of the material. The confinement effects lead to several commercially useful characteristics. From a processing viewpoint, nanostructured powders offer the potential for very high sintering rates at



This image shows Nano-Sized SiC Powders (magnified 120,000 times).

lower temperatures.

In order to reduce the concept of this new technology to practice, the innovators focused on β -SiC and continuous SiC fiber-reinforced SiC composites. Nanoceramic powders were produced and then formed into monoliths. These monoliths were dispersed into the fibers by several alternative methods, isostatically compacted, and hot pressed to achieve high densities.

Nano-sized SiC powders synthesized were characterized using x-ray diffraction and transmission electron microscopy. The nano-sized SiC powders were further characterized using the B.E.T. method, and surface area was found to be 100 m²/g. Using 3.2 g/cm³ as the density of SiC, the average powder size was calculated as 9.4 nm.

The pressureless sintering was carried out in a high-temperature graphite furnace. The graphite heating element is insulated from the water-cooled stainless steel chamber. A EURO-CUBE 425 Thyristor unit was used to precisely control the furnace

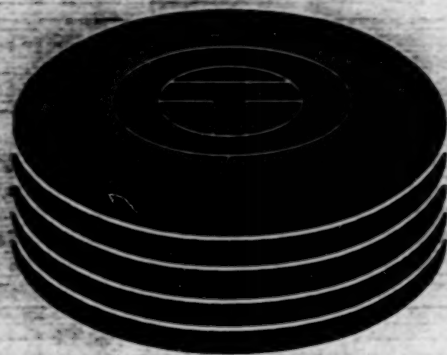
temperature and heating/cooling cycle. The chamber was first pumped down to ~10 torr using a mechanical pump, then flashed with argon three times. Either an argon or argon-reducing atmosphere was used during the sintering process.

Rapid densification technology will be of great value in the development of new ceramic-matrix-composite technologies of the future.

With 10-nm-sized SiC nanopowders, monolithic SiC and SiC matrix composite samples were pressureless sintered to over 90 percent of the theoretical density in 240 minutes at 1,450 and 1,500 °C respectively. At temperatures such as those presently used in conventional SiC and SiC/SiC densification practices (>2,000 °C), the densification of nano-sized SiC and SiC/SiC is expected to be more than 30 times faster. Beyond processing benefits, the invention offers performance benefits as well. The densified composite samples prepared with nano-sized SiC, for example, offer much higher fracture strength (400 percent) than those prepared with micron-sized SiC as starting powders. This technology breakthrough is applicable to other commercially important carbide, nitride, boride, silicide, and oxide ceramic compound compositions as well.

This work was done by Mark Liu Yang and Tapesha Yadav, Nano-materials Research Corporation, for the Marshall Space Flight Center. Further information is contained in a TSP [see page 1].

Inquiries concerning rights for the commercial use of this invention should be addressed to the Patent Counsel, Marshall Space Flight Center [see page 1]. Refer to MFS-26458.



Computer Programs

Machinery

35 Program Computes Equilibrium Compositions of Mixtures

Computer Programs

These programs may be obtained from COSMIC. Please contact

COSMIC®

Computer Services Annex
University of Georgia
Athens, GA 30602
Telephone No. (404) 542-3265.

Machinery

Program Computes Equilibrium Compositions of Mixtures

This program can be applied to a variety of problems in chemistry and chemical engineering.

The Chemical Equilibrium with Applications (CEA) computer program is used to obtain chemical-equilibrium compositions of complex mixtures. This program can be applied to a wide vari-

ety of problems in chemistry and chemical engineering. Specifically, CEA is applicable to the following kinds of problems:

1. Obtaining chemical-equilibrium compositions for assigned thermodynamic states;
2. Calculating theoretical performance of a rocket with a combustion chamber of finite or infinite area;
3. Calculating Chapman-Jouguet detonations; and
4. Calculating shock-tube parameters for both incident and reflected shocks.

CEA requires two types of input. The first type is of thermodynamic data and thermal-transport-property data for individual species. These data accompany the program but the user can modify them. Approximately 1,340 reaction products and 60 reactants are included in the thermodynamic-data file. The second type comprises seven categories of problem-input data prepared by the user. These data are grouped into input sets in a general free format.

The program prints five kinds of output:

the input data for the given problem, tables of results, files for plotting, information concerning iterative procedures, and other intermediate output. To facilitate addition or deletion of applications of the program, CEA is organized into eight modules. Fourteen example problems and the corresponding outputs are included.

CEA is written in ANSI standard FORTRAN 77 to be machine-independent. A FORTRAN 77 compiler is required. CEA has been successfully implemented on a '586-class IBM personal computer running Windows 95/NT 4.0, an HP9000/720 computer running HP-UX 9.03, and an SGI IRIS Indigo2 computer running IRIX 6.2. The standard distribution medium for CEA is one 3.5-in. (8.89 cm), 1.44MB, MS-DOS-format diskette. Alternate distribution media are available on request. CEA was released to COSMIC in 1998.

*This program was written by Bonnie J. McBride of **Lewis Research Center** and Sanford Gordon, Consultant. For further information, see TSP's [page 1].*
LEW-16645

BLANK PAGE



Mechanics

Hardware, Techniques, and Processes

- 39 Replaceable Windows With Alignment and Sealing Features
- 39 Latching Devices for Electrical and Mechanical Connections
- 40 Penetrator Projectile Tolerates Some Misalignment
- 41 Robot Hands With Electroactive-Polymer Fingers

BLANK PAGE

Replaceable Windows With Alignment and Sealing Features

Installation and removal can be accomplished without tools.

Lewis Research Center,
Cleveland, Ohio

Window assemblies (see figure) have been developed to satisfy special requirements pertaining to ease of replacement, alignment, sealing, and resistance to vibration in a spaceborne laboratory apparatus for experiments on combustion in microgravity. These window assemblies are also well suited to a variety of terrestrial applications; for example, they could be used as observation ports or as mechanical or electrical feedthrough devices on industrial process chambers, vacuum chambers, or oceanographic equipment.

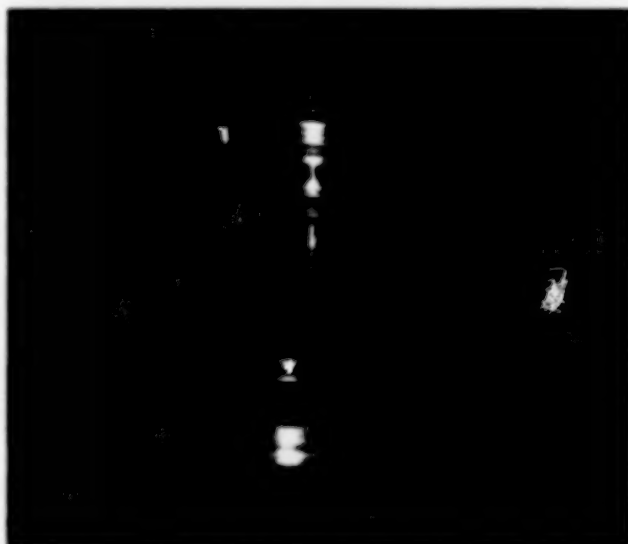
The windows can be installed and removed manually, without tools. Each window mates with a seat that is a permanent part of the chamber in which the window is to be installed. All one need do to install a window is to align it approximately with the seat, then rotate the window one turn. The rotation brings the window into alignment, brings sealing surfaces together to make a vacuum- or pressure-tight seal, and provides a vibration-proof connection. The window gives a firm feel when it becomes seated.

This mode of operation of the window is established by a unique combination of threads, sealing features, and a ratchet. A multiple-lead acme thread ensures an easy start. Because the seal acts on a bore in the chamber wall, instead of on a face parallel to the plane of the window, there is no need for the large clamping force that would be needed for a face seal. The ratchet includes a spring-loaded dimple plate acting on tapered lands. The lands are cut steeper in the window-removal than in the window-installation direction, so that more torque is needed to remove than to install the window; this feature helps to prevent loosening in the presence of vibrations.

This work was done by Malcolm Robbie of Aralex Corp. and Raymond Hornyk of ADF for **Lewis Research Center**. Further information is contained in a TSP [see page 1].



Window Assembly Showing Handle (in Green) Folded Up for Installation



Window Assembly Showing Acme Thread and Sealing Surfaces

No Tools Are Needed to install or remove these windows, which are simply inserted in approximate initial alignment, then rotated to obtain precise alignment and tight seals. Windows can be used for observation or as feedthrough devices.

Inquiries concerning rights for the commercial use of this invention should be addressed to NASA Lewis Research Center, Commercial Technology Office,

Attn: Tech Brief Patent Status, Mail Stop 7-3, 21000 Brookpark Road, Cleveland, Ohio 44135. Refer to LEV-16529.

Latching Devices for Electrical and Mechanical Connections

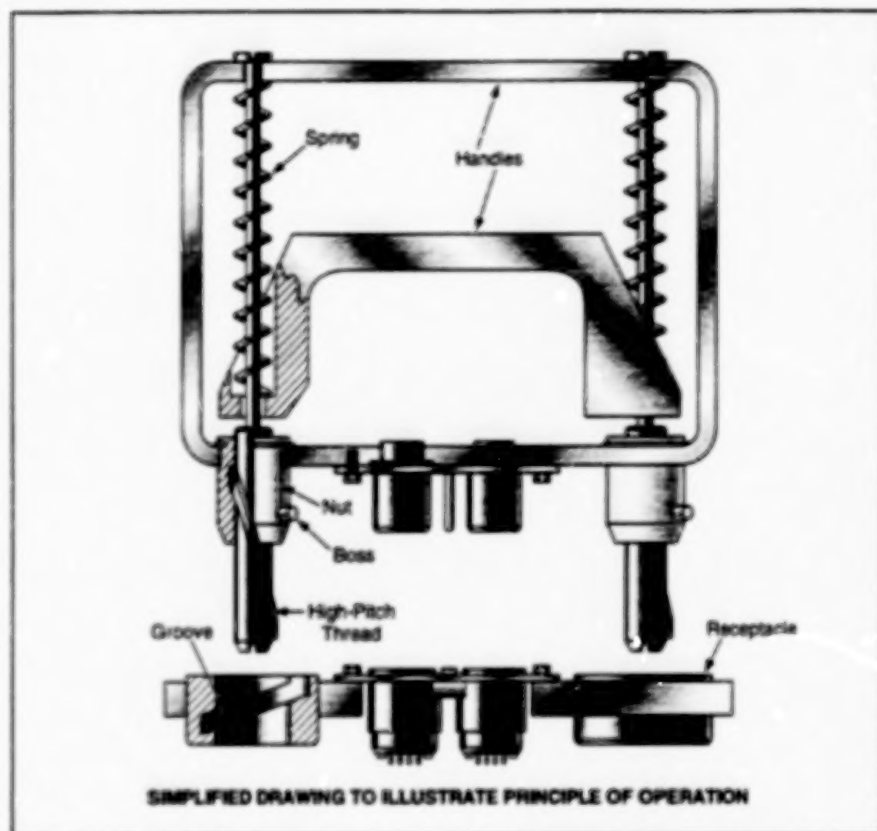
Connections can be made or broken quickly by simple hand motions, without tools.

Lewis Research Center,
Cleveland, Ohio

Latching devices have been developed to provide electrical connections, secure mechanical and thermal connections, and

optical alignment for mounting electronically controlled cameras on the spaceborne laboratory apparatus described in

the preceding article. Traditionally, the installation of such a camera or a similar instrument has been a time-consuming



The Two Mating Subassemblies can be connected and disconnected quickly by simple hand motions.

task that involved tightening of multiple fasteners to specified torques, making separate electrical connections, and use of special tools. The present latching devices are designed for quick connection and quick disconnection by simple manual hand motions; no tools are needed. These latching devices could also be used on Earth in numerous industrial and scientific applications to provide electrical, mechanical, thermal, and/or optical inter-

connections that can be made and broken quickly and reliably, without tools.

Each latching device comprises two mating subassemblies (see figure). The operation of the latching device depends on a unique combination of threaded parts. The inner spring-loaded handle is connected to the rods, which are not free to rotate. A single high-pitch thread on each rod engages a nut that is free to rotate but not to translate along its axis of rotation. A boss

on each nut engages a lower-pitch groove in its mating receptacle, each of which is free to rotate with respect to the handle.

To connect the two subassemblies, one simply squeezes together the two spring-loaded handles on one subassembly, inserts the rods and nuts protruding from that subassembly into mating receptacles on the other subassembly, then releases the handles. The initial squeezing of the handles causes the nuts to rotate to an angular position in which the bosses on the nuts are aligned with the openings to the grooves in the receptacles. The release of the handle causes the nuts to rotate in a direction to make the bosses slide along the grooves deeper into the receptacles, thereby drawing the two subassemblies together at a common surface. In the original application, the contact at the common surface brings the camera into alignment with an optical reference surface. The force clamping the two subassemblies together is generated by the spring and multiplied by a mechanical advantage proportional to the ratio between the pitch of the thread and the pitch of the groove. By use of low-friction coating material on the threads, grooves, and bosses, the achievable clamping force can be made to approach the ideal clamping force more closely.

This work was done by Malcolm Robbie of Analox Corp. for Lewis Research Center. Further information is contained in a TSP [see page 1].

Inquiries concerning rights for the commercial use of this invention should be addressed to NASA Lewis Research Center, Commercial Technology Office, Attn: Tech Brief Patent Status, Mail Stop 7-3, 21000 Brookpark Road, Cleveland, Ohio 44135. Refer to LEW-16528.

Penetrator Projectile Tolerates Some Misalignment

A forebody/afterbody design prevents buckling and ensures penetration.

A two-body design has enabled an instrumented penetrator projectile to function with increased tolerance to initial misalignment among (a) the longitudinal axis of the penetrator, (b) the velocity of impact on the ground, and (c) the local perpendicular to the surface at the point of impact. In the original application, the two-body penetrator will be launched from a spacecraft to impinge on Mars, where it will sample the soil. The two-body penetrator design is easily adaptable to instrumented penetrators for sampling subsurface materials in

sand, soil, mud, snow, or ice in hostile or inaccessible environments on Earth.

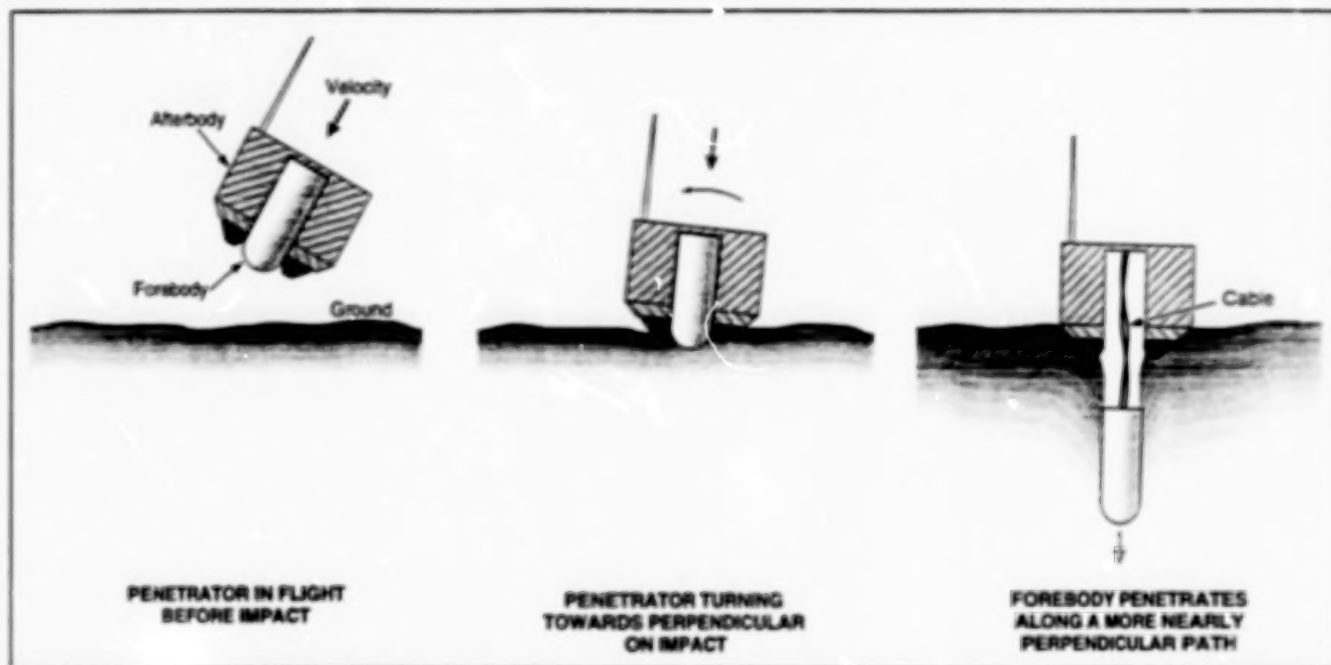
Older instrumented-penetrator designs feature unitary bodies that are much longer than they are wide. In a typical case, if the longitudinal axis of the body deviates from impact velocity direction by an angle of more than about 6°, then the penetrator buckles and/or fails to penetrate.

The two-body penetrator (see figure) includes a forebody and an afterbody. The forebody contains the instrumentation and machinery required to penetrate the ground; the forebody has a

hemispherical tip and is shorter and stubbier, in comparison to a typical older unitary penetrator. The afterbody contains batteries, radio-communication circuitry, and those sensors (e.g., a Sun sensor and an atmospheric-pressure sensor) that must not penetrate the ground. Prior to impact, the forebody is stowed in a longitudinal cylindrical recess in the afterbody.

Upon impact, a flange on the bottom of the afterbody becomes braked upon contact with the ground. The braking action is such that in the presence of misalignment,

NASA's Jet Propulsion Laboratory,
Pasadena, California



The **Afterbody** is **Braked and Turned** upon impact to face more directly down into the ground. The forebody separates from the afterbody and penetrates a short distance below the surface.

the afterbody turns so that the recess holding the forebody becomes aligned more nearly perpendicularly to the ground surface. As the afterbody decelerates, the forebody slides out of the recess, penetrating the ground underneath the afterbody. The forebody and afterbody remain connected by a flexible cable that pays out from the forebody during impact.

The concept has been tested in experiments in which two-body penetrators were fired from an air gun into sand, soil, and cement-mix targets at speeds from 168 to 208 m/s. In one test in which a penetrator was fired into the ground at an angle of 75° with the surface, the forebody was found to have traveled into the soil at an angle of 83° with the sur-

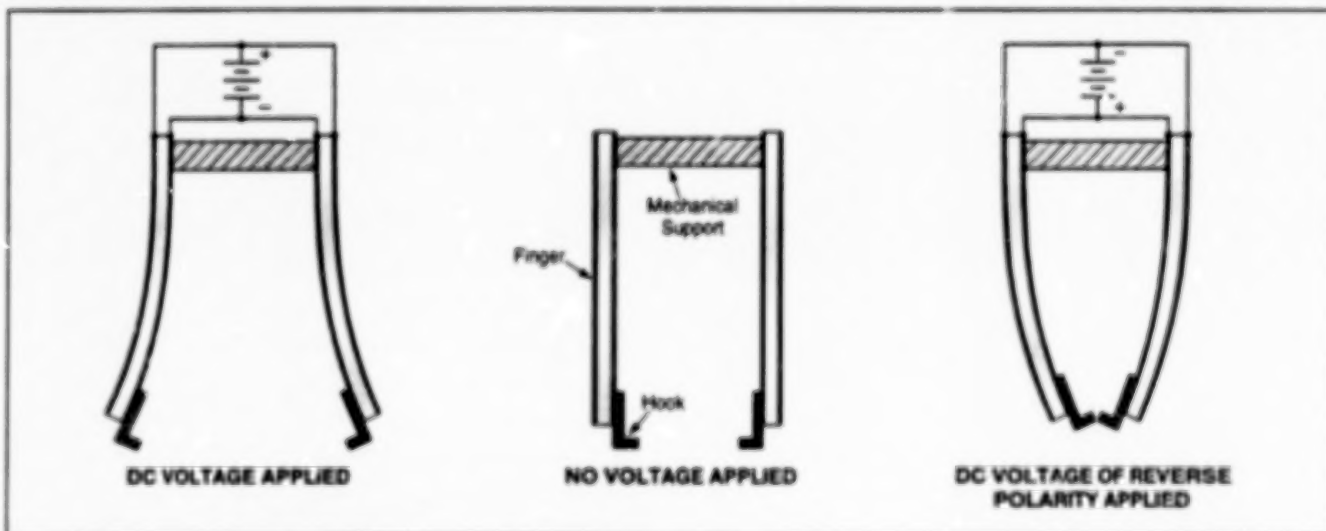
face; that is, more nearly perpendicularly to the surface, as intended.

This work was done by Donald Bickler and Tommaso Rivellini of Caltech for NASA's Jet Propulsion Laboratory. Further information is contained in a TSP [see page 1].
NPO-20295

Robot Hands With Electroactive-Polymer Fingers

The fingers function similarly to human fingers.

NASA's Jet Propulsion Laboratory,
Pasadena, California



Electroactive Polymeric (Ionomeric) Fingers Bend by virtue of the electrostrictive effect in response to applied voltage. The direction of bending depends on the polarity of the voltage.

Multifinger electroactive-polymer grippers (MEPGs) are simple, compact, lightweight robotic end effectors with fingers

that bend and function similarly to human fingers. The fingers are made from electroactive polymers, which are well suited to

use in bending-type actuators because they can be formed into various shapes, are flexible and tough, and damp vibra-

tions. In comparison with electroactive ceramics, electroactive polymers are much lighter and exhibit about 100 times as much actuation strain. Like other polymers, electroactive polymers can be mass-produced at relatively low cost.

More specifically, the fingers of MEPGs are made from ion-exchange membrane platinum (IEMP) composite polymers. When a voltage is applied across the thickness of such a finger, electrostriction in the polymer causes the finger to bend; the direction of bending depends on the polarity of the voltage.

The figure illustrates an MEPG with two opposed fingers wired in antiparallel so that they will bend in opposite directions (and thus toward or away from each other) in response to an applied voltage. The angle

of bending of a finger can exceed 120°. Typically, a finger is driven with a potential of about 5 V and consumes a power of about 25 mW.

In a typical operational sequence, a voltage of one polarity is applied to spread the fingers apart to clear an object as the hand approaches the object. Once the hand is positioned over the object with a finger on each side, the polarity is reversed to close the fingers around the object. Hooks on the ends of the fingers (somewhat analogous to fingernails) help to secure the grip on the object, which can be picked up and carried once the fingers close around it. In experiments, a two-finger prototype hand lifted a rod with a mass of 1.5 g, and a four-finger prototype hand lifted a rod with a mass of 10.3 g.

This work was done by Yoseph Bar-Cohen, Tianji Xue, Mohsen Shahinpoor, and Shyh-Shiuh Lih of Caltech for NASA's Jet Propulsion Laboratory. Further information is contained in a TSP [see page 1].

In accordance with Public Law 96-517, the contractor has elected to retain title to this invention. Inquiries concerning rights for its commercial use should be addressed to

Technology Reporting Office

JPL

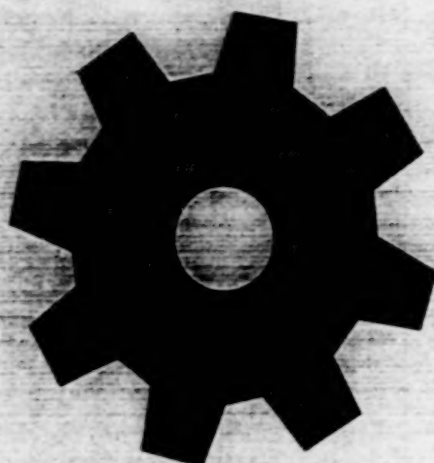
Mail Stop 122-116

4800 Oak Grove Drive

Pasadena, CA 91109

(818) 354-2240

Refer to NPO-20103, volume and number of this NASA Tech Briefs issue, and the page number.



Machinery

Hardware, Techniques, and Processes

- 45 Vacuum Three-Ball Tribometer for Testing Liquid Lubricants

Books and Reports

- 46 Sorption Compressor for Collecting Atmospheric CO₂ on Mars
46 Mars Lander

Vacuum Three-Ball Tribometer for Testing Liquid Lubricants

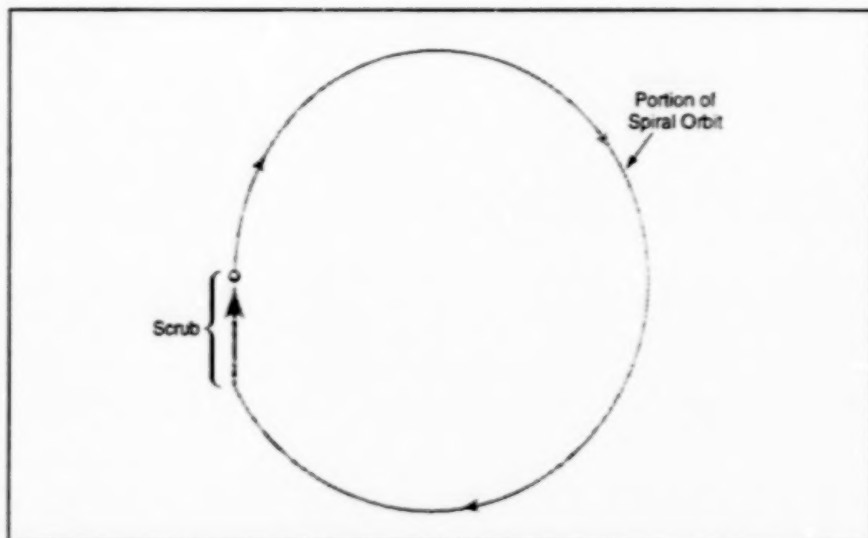
Tribodegradation of lubricants can be studied under controlled, realistic conditions.

Lewis Research Center,
Cleveland, Ohio

A three-ball tribometer has been developed for use in evaluating the performances of oils and greases as lubricants in a vacuum at room temperature. This apparatus differs from the one described in "Vacuum Four-Ball Tribometer for Testing Liquid Lubricants" (LEW-16194), NASA Tech Briefs, Vol. 21, No. 4 (April 1997), page 64. The present apparatus is designed especially for experiments on the tribodegradation of liquid lubricants under conditions similar to those observed in preloaded angular-contact ball bearings operating in the boundary-lubrication regime in a vacuum. Tribodegradation can include both physical and chemical changes caused by a combination of contact stresses and aggressive ambient conditions. The chemical changes typically involve chemical reactions between lubricants and bearing surfaces, decomposition of lubricants, and darkening of lubricants associated with the formation of products denoted generally as "friction polymers."

The tribometer is housed in a stainless steel vacuum chamber. The main tribological assembly is a retainerless steel thrust bearing with three balls of 0.5-in. (12.7-mm) diameter placed symmetrically between flat races. The balls and plates are made of 440C stainless steel, which is commonly used in instrument ball bearings. The bottom plate is mounted on a shaft that passes out of the vacuum chamber through a steel bellows and is connected via a load cell to a deadweight cantilever device that pushes the bottom plate upward to apply the preload. A preload of 100 lbf (445 N) provides a mean Hertz (contact) stress of 1.39 GPa, which is typical for a preloaded instrument bearing. The bottom plate does not rotate. Driven by a synchronous gearmotor via a ferrofluidic rotary feedthrough, the top plate rotates at 4 rpm. Such a low speed helps to ensure the desired room-temperature test condition.

The rotation of the top plate causes the balls to roll on the bottom plate in an almost circular orbit of about 21-mm radius. More precisely, the balls gradually spiral outward from their initial radii with a pitch of about 0.5 mm per revolution and would eventually fall out if allowed to continue rolling without the restraint provided



The Balls Move in a Stable Orbit comprising spiral and scrub portions, the dynamics of which are not yet well understood. Further study of the dynamics is expected to contribute to understanding of liquid-lubricated rolling friction.

by a guide plate. The balls eventually make contact with the guide plate for a distance of about 5 mm, where they move along a straight line called the "scrub" and are forced back to the initial, slightly smaller orbit radius. Together, the spiral and scrub portions of the orbit constitute a track (see figure) that is stable and repeatable and is traversed thousands of times by the balls during an experiment. The scrub is also utilized to measure the coefficient of friction; this measurement is accomplished by use of a load cell that supports the guide plate and measures the force exerted on the guide plate by each passing ball. To ensure that bulk temperatures remain near room temperature and to prevent metallic wear, an experiment is stopped at the first sign of increased friction.

Once the vacuum chamber has been evacuated and an experiment is in progress, a residual-gas analyzer with a line of sight to the balls and plates is used to determine the composition of residual gas from the chamber and of any molecular species that evolve through tribodegradation of the lubricant. After an experiment, the degraded lubricant can easily be examined by use of such surface- and thin-film-analysis techniques as optical and electron microscopy, photoelectron spectroscopy, and infrared and Raman microspectroscopy.

The design of this tribometer offers sev-

eral advantages. It provides a more credible simulation of preloaded angular-contact ball bearings operating in the boundary-lubrication regime than does a tribometer containing a ball sliding on a plate. Retainerless operation eliminates forces associated with balls sliding in retainer pockets and thereby enables a simple yet rigorous analysis of stresses to which a lubricant is subjected. The absence of a porous retainer eliminates the uncertainties associated with a supply of lubricant; the bearing is forced to operate with an extremely small lubricant charge, so that there is maximum opportunity for the lubricant to be tribologically exercised to make it undergo tribodegradation. The balls and plates are inexpensive. Surface analyses of tracks can be performed more easily on the flat plates of this tribometer than on the curved surfaces of ordinary bearing races.

This work was done by Stephen V. Pepper and Ben T. Ebihara of Lewis Research Center and Edward Kingsbury of Interesting Rolling Contact. Further information is contained in a TSP [see page 1].

Inquiries concerning rights for the commercial use of this invention should be addressed to NASA Lewis Research Center, Commercial Technology Office, Attn: Tech Brief Patent Status, Mail Stop 7-3, 21000 Brookpark Road, Cleveland, Ohio 44135. Refer to LEW-16550.

Books and Reports

Sorption Compressor for Collecting Atmospheric CO₂ on Mars

A report describes a small, lightweight sorption compressor that is now undergoing development for use in collecting CO₂ from the atmosphere on Mars. This compressor would be part of a system that would use the CO₂ to generate oxygen and a carbon-based fuel for a spacecraft to return specimens to Earth. Unlike mechanical compressors, a sorption compressor has few moving parts and thus has potential for greater reliability. The sorbent material in the developmental compressor is a zeolite, which preferentially adsorbs CO₂ over other Martian atmospheric gases when cooled to the Martian nighttime temperature of about

200 K. During the Martian daytime, when solar power would be available, the sorbent would be heated in a closed volume to desorb and pressurize the CO₂ for use elsewhere in the system. It should be possible to use waste heat to heat the sorbent during desorption, thereby increasing the energy-conversion efficiency of the system. It should also be possible to exploit the large Martian daily temperature swing to achieve a further increase in efficiency.

This work was done by Donald Rapp and Paul Karlmann of the California Institute of Technology for NASA's Jet Propulsion Laboratory. To obtain a copy of the report, "Adsorption Compressor for Acquisition and Compression of Atmospheric CO₂ on Mars," see TSP's [page 1].

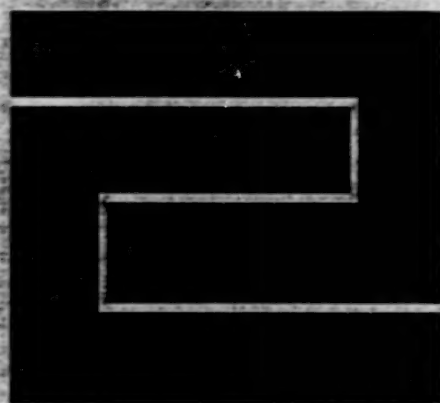
JPO-20353

Mars Lander

A brief report presents drawings for the conceptual design of a spacecraft that would land on Mars or another remote planet. The spacecraft would have a tetrahedral shape, would include airbags to cushion impact, and would have a self-righting capability. The drawings show the general appearance of the spacecraft and show the outlines and locations of some power, propulsion, temperature-regulation, and communication equipment. This design presents significant licensing opportunities in the toy and model industries.

This work was done by Tommaso P. Rivellini, Robert Bamford, Jim Hendrickson, and Mike O'Neal of Caltech for NASA's Jet Propulsion Laboratory. For further information, see TSP's [page 1].

NPO-19859



Fabrication Technology

Hardware, Techniques, and Processes

- 49 Improved Packaging of Silica Optical Fibers in Sensor Heads
- 49 Fabricating Refractory-Metal Solar-Engine Components by VPS
- 50 Fabrication of Diffractive GaAs Microlenses

BLANK PAGE

Improved Packaging of Silica Optical Fibers in Sensor Heads

Fibers would be held in metal ferrules by matrices of fused glass.

Lewis Research Center,
Cleveland, Ohio

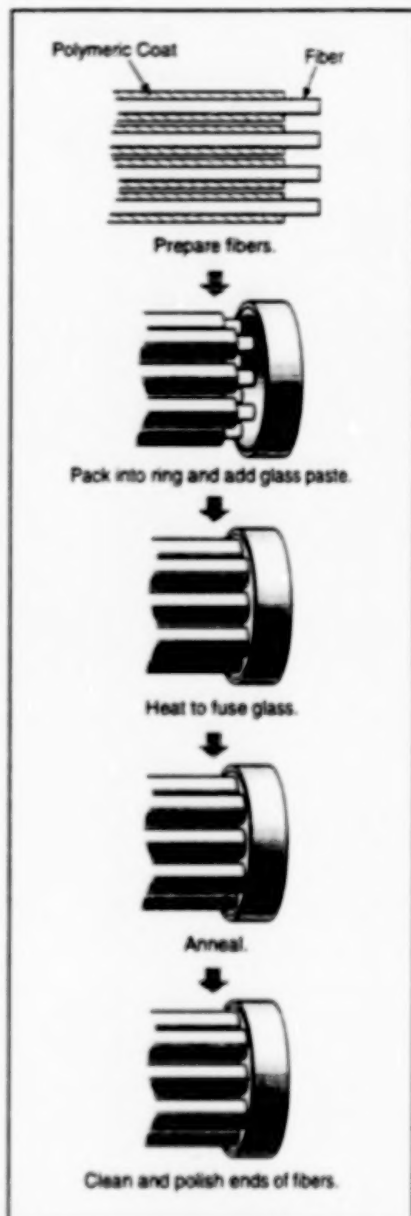
A process for the fabrication of improved high-temperature fiber-optic sensor heads has been proposed. Fiber-optic sensor heads that can withstand hot, dirty, noisy environments are needed for advanced jet engines and stationary power-generating turbine engines.

A typical optical fiber for high-temperature service is made of fused silica. Also typically, the surface layer of the fiber is doped with germanium to alter its index of refraction in such a way as to achieve a specific numerical aperture needed for directionally selective sensing. Engine operating temperatures to which silica optical fibers are likely to be exposed range up to somewhat above 250 °C, and the fibers can withstand higher temperatures up to 700 °C. Prolonged exposure to temperatures above 700 °C causes diffusion of germanium from the surface layers into the pure fused silica cores of the fibers, with consequent loss of the desired numerical apertures. Accordingly, any heating that must be performed in fabricating a sensor head should be limited to temperatures below 700 °C.

A fiber-optic sensor is made with multiple optical fibers to provide (1) a cross-sectional area large enough for reliable sensing and (2) redundancy for protection against breakage of one or more fiber(s). To form a sensor head, the fibers are bundled at one end, where they are sealed rigidly and hermetically in a ring sized to fit an instrumentation port in an engine. The ring is made of Kovar (or equivalent) iron/nickel/cobalt alloy.

The proposed fabrication process would include a step for sealing the fibers into the ring by use of a glass that melts at a temperature below 700 °C. The process (see figure) would comprise the following steps:

1. Prepare the requisite number of silica fibers of equal length. Such fibers are



Silica Optical Fibers Would Be Sealed into a metal ring by applying a paste of low-melting-temperature glass, then fusing the glass.

supplied with polyimide or nylon coats. Strip off about 1 in. (about 2.5 cm) of the coat at one end of each fiber. The polymeric coating material will not survive the high temperature to which the stripped ends will subsequently be exposed, but elsewhere than at the stripped ends it provides mechanical support and thus should be left intact.

2. Pack the fibers in the ring. Fill the interstices between fibers and the space between the fibers and the ring with a boron-glass paste. If necessary, install fixtures to hold the fibers steady in the ring.
3. Using a controllable source of heat, raise the temperature of the glass paste to at least the melting temperature of the boron glass (580 °C) but no more than 700 °C. Continue heating until the paste fuses and bonds to the fiber surfaces.
4. Anneal the package by bringing down the temperature very slowly. Prolonged heating at intermediate temperatures (e.g., 500 °C) might be necessary to prevent cracking.
5. Clean off excess glass and polish the ends of the fibers in the ring. The other ends of the fibers can be bundled as a conventional fiber-optic cable because they will not be exposed to high operating temperatures.

This work was done by E. Shu, W. Daum, and L. Petrucco of General Electric Co. for Lewis Research Center. Further information is contained in a TSP [see page 1].

Inquiries concerning rights for the commercial use of this invention should be addressed to NASA Lewis Research Center, Commercial Technology Office, Attn: Tech Brief Patent Status, Mail Stop 7-3, 21000 Brookpark Road, Cleveland, Ohio 44135. Refer to LEW-16264.

Fabricating Refractory-Metal Solar-Engine Components by VPS

Little or no ancillary machining is necessary.

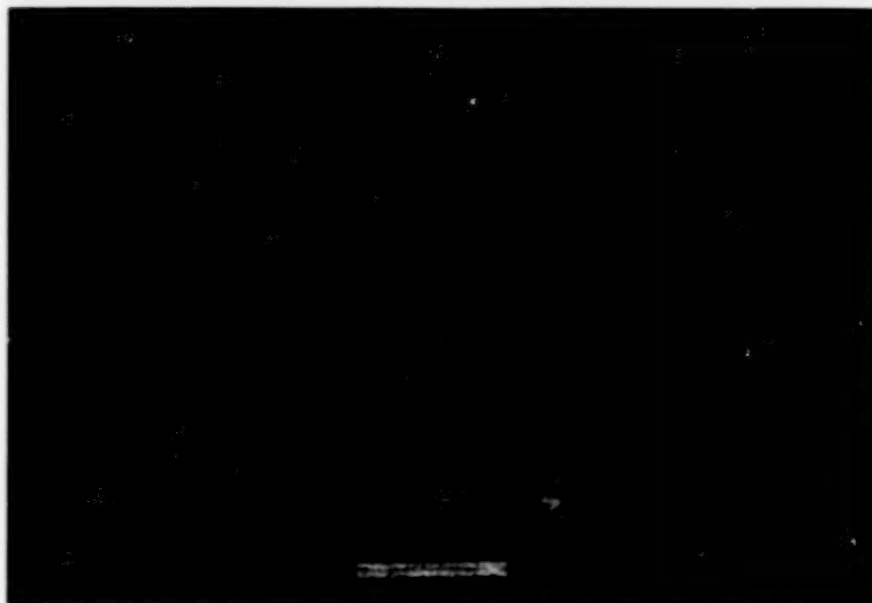
Marshall Space Flight Center,
Alabama

Vacuum plasma spraying (VPS) has been demonstrated to be an effective technique for the fabrication of refractory-metal components of solar-thermal engines. Heretofore, such components have been fabricated by specialized tech-

niques that include electrical-discharge machining, shear spinning, sintering under pressure, chemical vapor deposition, and electrochemical machining. Though effective, these specialized techniques are time-consuming and costly.

On the other hand, VPS makes it possible to fabricate components with complex shapes, simply and at relatively low cost.

VPS is a thermal-spray process conducted in a low-pressure, inert-gas atmosphere. A hot plasma is generated by



Vacuum Plasma Spraying was used to make all of these parts except the flange with holes. The item at the right comprises three concentric shells.

making an inert gas flow through a direct-current arc. The plasma flows through a nozzle to a downstream vacuum chamber, where the pressure is maintained at about 100 torr (about 13 kPa) and the deposition substrate is located. A powder of the material to be deposited is injected into the plasma, causing the material to be heated and accelerated toward the substrate. The process is continued until the deposit reaches the desired thickness.

In the present application of VPS, the substrates used to form solar-thermal-engine components are graphite mandrels. Each mandrel acts as a male mold to form the inside of the deposit to the required size, shape, and surface finish. Inasmuch as graphite is soft and easy to

machine, complex shapes and precise surface textures can be achieved without difficulty. For example, helical flow channels for transfer of heat to a working fluid can be formed integrally into a component of a generally cylindrical absorber cavity (see figure), and textures necessary for maximizing absorption of solar radiation can be imparted to the inner surface of the cavity by the outer surface of the mandrel used to make the innermost component.

After the refractory metal has been deposited to the desired thickness, the mandrel is removed by blasting with acrylic or other polymeric beads, which are hard enough for eroding the graphite but soft enough not to damage the refractory-metal deposit. Removal of the graphite in

this manner is rapid and simple and complies with environmental laws.

Because the interior of a component formed by VPS is inherently of net size, shape, and surface finish imparted by the mandrel, no additional machining or surface conditioning of the interior is necessary. The exterior dimensions can be controlled by controlling the deposition rate and time, so that the exterior of the VPS-formed component is near net size and shape. Thus, little or no subsequent machining is necessary; this is especially advantageous for fabricating components of tungsten, rhenium, and molybdenum, which are difficult to machine by conventional techniques. Even in cases in which tolerances are tighter than are achievable by VPS, the amount of subsequent machining and grinding needed is less than in older methods and is confined to exterior surfaces, which are more accessible than interior surfaces are. While VPS shares these advantages with other vacuum-vapor-deposition processes (chemical vapor deposition and physical vapor deposition), VPS deposits materials at rates orders of magnitude greater than those of the other processes.

This work was done by Frank R. Zimmerman, D. Andy Hissam, and Harold P. Gerrish of **Marshall Space Flight Center** and William Davis of Boeing North American. Further information is contained in a TSP [see page 1].

Inquiries concerning rights for the commercial use of this invention should be addressed to the Patent Counsel, Marshall Space Flight Center [see page 1]. Refer to MFS-31242.

Fabrication of Diffractive GaAs Microlenses

Relief patterns are made by electron-beam lithography, then transferred by plasma etching.

A planar array of microscopic diffractive optical elements that resemble macroscopic Fresnel lenses can be fabricated as an array of continuous relief patterns on a GaAs substrate by a procedure that includes the transfer of a corresponding array of patterns formed on a surface layer of poly(methyl methacrylate) (PMMA) by electron-beam lithography. The diffractive optical elements could be, for example, microlenses on back-side-illuminated imaging arrays GaAs-based quantum-well infrared photodetectors (these microlenses are used to concentrate incident infrared light into sub-pixel-size active device

areas). The fabrication procedure is not limited to arrays of microlenses; it can also be adapted to making other optical elements (for example, holograms or diffractive microlenses) in GaAs.

A GaAs substrate to be patterned is first coated with PMMA to a suitable thickness (e.g., 2 μm). A pattern corresponding to an approximation of the desired surface relief pattern on GaAs is written in the PMMA by a scanning electron-beam apparatus, with local electron-beam dosage pixelized on a grid of suitably high resolution (e.g., 1- μm -square cells). The local electron-beam dosage to the PMMA must be varied to

NASA's Jet Propulsion Laboratory,
Pasadena, California

obtain the desired final local variation of surface height of the GaAs substrate, taking account of the effects of subsequent processing steps, including such complicating effects as nonlinear dose-vs.-depth relationships and back-scattering of the electron beam from previously written nearby areas. The exposed PMMA is then developed by spinning the coated substrate and spraying acetone down onto it, yielding an intermediate surface relief pattern on the PMMA. The total development time is usually about 10 seconds, and depths are usually accurate to within ± 5 percent.

The surface relief pattern on the PMMA is transferred to the underlying GaAs by plasma etching. The PMMA-coated substrate is placed in an electron-cyclotron-resonance system, wherein it is cooled to 10 °C and etched, using Ar and BCl₃ as process gases. The chosen combination of process gases and physical processing conditions yields an advantageously high GaAs/PMMA etch ratio.

This work was done by Frederick Pool, Daniel Wilson, Richard Muller, and Paul Maker of Caltech for NASA's Jet Propulsion Laboratory. Further information is contained in a TSP (see page 1).

In accordance with Public Law 96-517, the contractor has elected to retain title to this invention. Inquiries concerning rights for its commercial use should be addressed to

*Technology Reporting Office
JPL
Mail Stop 122-116
4800 Oak Grove Drive
Pasadena, CA 91109
(818) 354-2240*

Refer to NPO-20303, volume and number of this NASA Tech Briefs issue, and the page number.

BLANK PAGE



Mathematics and Information Sciences

Hardware, Techniques, and Processes

55 Localization by Maximum-Likelihood Matching of Range Maps

BLANK PAGE

Localization by Maximum-Likelihood Matching of Range Maps

This technique is intended for use in autonomous navigation of robotic vehicles.

NASA's Jet Propulsion Laboratory,
Pasadena, California

A procedure for determining the location of an instrumentation platform on natural terrain is based on a concept of maximum-likelihood matching of two range maps: (1) a local range map generated by processing of images of the terrain in the immediate vicinity acquired by stereoscopic video cameras mounted on the platform and (2) a previously generated range map of a larger surrounding terrain area (a "global" map) in a known frame of reference. The procedure, which is still undergoing testing and refinement, was developed primarily to aid the autonomous navigation of exploratory robotic vehicles on distant planets. The procedure might also be adaptable to similar applications on Earth and to such related applications as enabling blind persons to determine their locations in previously mapped natural and artificial environments.

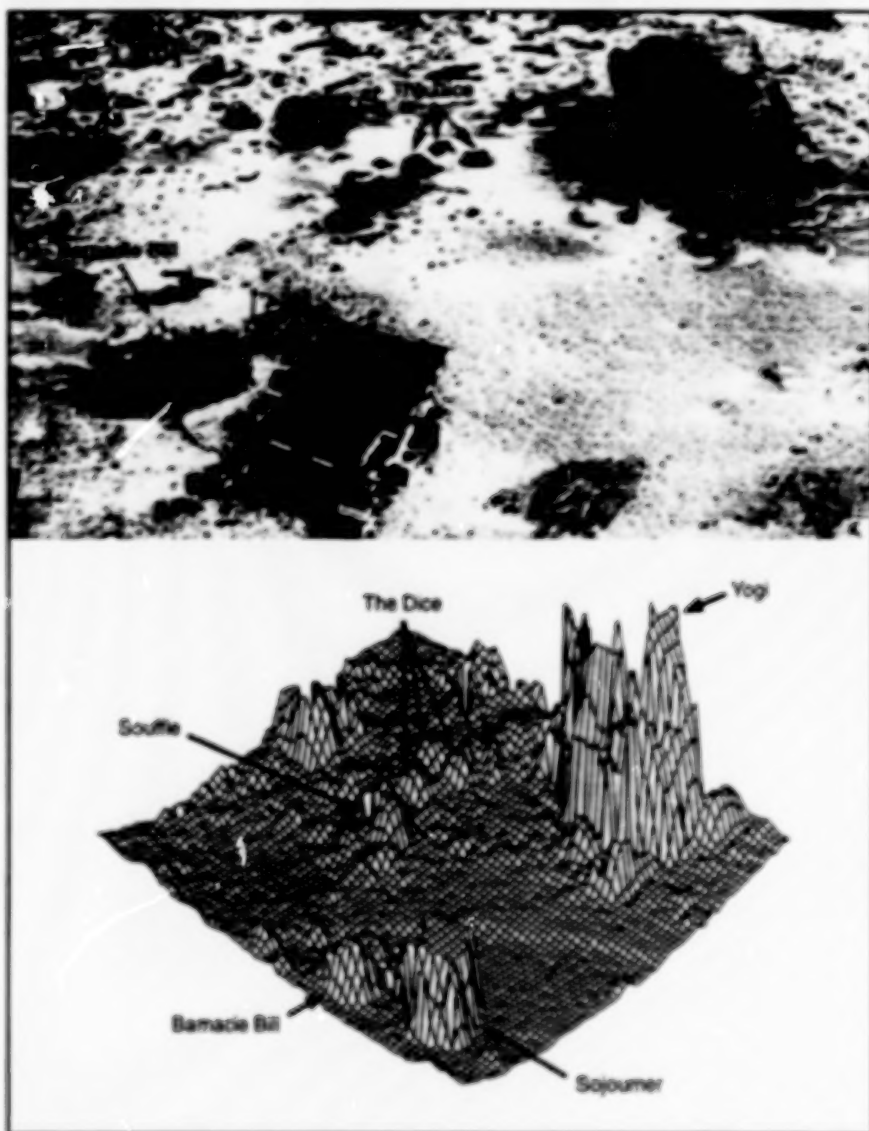
Once the local range map has been computed from the stereoscopic imagery, it is converted to a volume-cell (voxel) representation (see figure). Optionally, if the orientation of the robotic vehicle or other instrumentation platform is known from a gyrocompass, Sun sensor, or other independent sensor, then the conversion to the voxel representation can include rotation into the orientation of the global map to facilitate matching.

The range points in the local map are binned in a three-dimensional occupancy map of the surroundings at some specified scale. In a subprocess that amounts to high-pass filtering of vertical-position data, the local average of the terrain height is subtracted from each cell; this subprocess is not strictly necessary and it reduces the ability to determine changes in the height of the platform, but, advantageously, it reduces the computation time needed for localization by eliminating the need to search over vertical translations. Each cell in the occupancy map is said to be occupied or unoccupied, according to whether it contains or does not contain, respectively, a range pixel.

The degree of matching between the global map and the local occupancy map is quantified by use of conventional image-matching measure based on the Hausdorff distance and reformulated in probabilistic terms according to the principle of maximum-likelihood estimation. The likelihood function is given by

$$L(X) = \prod_{i=1}^n p(D_i; X),$$

where D_i is the distance from the i th occupied voxel in the local map to the closest



A Three-Dimensional Local Map of the local terrain was generated from images acquired by stereoscopic cameras in the Sojourner vehicle. In a test of the procedure described in the text of this article, the local map was then matched with a "global" map generated from images acquired by stereoscopic cameras in the Mars Pathfinder lander, from which the Sojourner had been deployed.

voxel in the global map, X is the trial position of the local map relative to the global map, $p(D_i; X)$ is a probability distribution function (PDF), and n is the number of occupied voxels. To some extent, the PDF can be chosen arbitrarily: One suitable choice is a simple two-value PDF that yields a measure equivalent to the Hausdorff fraction commonly used in matching images; a better (albeit more complex) choice is a normal distribution function with an additive term.

The most likely position of the local map relative to the global map [that is, the position, X , that maximizes $L(X)$] is taken to be the position of the platform. The search for

this position can be started from a position that has been either assumed or estimated by an independent navigation technique. The estimate of position is then progressively refined by use of efficient search techniques that provide for the recursive division of the search space into smaller cells and pruning of cells that cannot contain a position superior to the best known position.

This work was done by Clark F. Olson of Caltech for NASA's Jet Propulsion Laboratory. Further information is contained in a TSP, see page 1].
NPO-20392

National Aeronautics and
Space Administration



END

02\09\99